

Final State Interactions and Relativistic Effects
in the Quasielastic (E,E') Reaction

C.R. Chinn^{1,2}, A. Picklesimer², and J.W. Van Orden³

¹Department of Physics and Astronomy,
University of Maryland, College Park, MD 20742

²Physics Division
Los Alamos National Laboratory, Los Alamos, NM 87545

³Continuous Electron Beam Accelerator Facility
Newport News, VA 23606

FINAL STATE INTERACTIONS AND RELATIVISTIC EFFECTS IN THE
QUASIELASTIC (E,E') REACTION

C. R. Chinn^{1,2}, A. Picklesimer², and J. W. Van Orden³

¹ Department of Physics and Astronomy
University of Maryland, College Park, Maryland 20742

² Physics Division
Los Alamos National Laboratory, Los Alamos, New Mexico 87545

³ Continuous Electron Beam Accelerator Facility
Newport News, Virginia 23606

November, 1988

ABSTRACT

The longitudinal and transverse response functions for the inclusive quasielastic (e, e') reaction are analyzed in detail. A microscopic theoretical framework for the many-body reaction provides a clear conceptual (nonrelativistic) basis for treating final state interactions and goes far beyond simple plane wave or Hermitean potential models. The many-body physics of inelastic final state channels as described by optical and multiple scattering theories is properly included by incorporating a full complex optical potential. Explicit nonrelativistic and relativistic momentum-space calculations quantitatively demonstrate the importance of such a treatment of final state interactions for both the transverse and longitudinal response. Nonrelativistic calculations are performed using final state interactions based on phenomenology, local density models and microscopic multiple scattering theory. Relativistic calculations span a similar range of models and employ Dirac bound state wave functions. The theoretical extension to relativistic dynamics is of course not clear, but is done in obvious parallel to elastic proton scattering. Extensive calculations are performed for ^{40}Ca at momentum transfers of 410, 550 and 700 Mev/c. A number of interesting physical effects are observed, including significant relativistic suppressions (especially for R_L), large off-shell and virtual pair effects, enhancement of the tails of the response by the final state interactions, and large qualitative and even shape distinctions between the predictions of the various models of the final state interactions. None of the models is found to be able to simultaneously predict the data for both response functions. This strongly suggests that additional physical mechanisms are of qualitative importance in inclusive quasielastic electron scattering.

more sophisticated models yield disparate transverse predictions for a reasonable range of input assumptions. The trend of these models is away from the observed transverse response, but toward the observed longitudinal response. Moreover, there exists no parameter-free prediction of the complete transverse response, particularly in the region between the quasielastic and delta-resonance peaks. Until a unified and consistent description is produced, skepticism concerning simple calculations of the transverse quasielastic response must be maintained.

The observed longitudinal response is shifted to lower energy transfers at momentum transfers below approximately 400 MeV/c, relative to the value expected for quasielastic scattering, while the transverse appears near the expected quasielastic value. This feature is suggestive of contributions from long range correlations excited by longitudinal virtual photons. A number of calculations of the longitudinal response have been carried out in the context of the random phase approximation (RPA) and these have been successful in providing a qualitative description of the longitudinal response at low momentum transfers.⁶ These calculations also predict some additional shifts and screening effects in both response functions at momentum transfers above those where the need for such long range correlations is obvious in the data. With the exception of those calculations which use the second RPA (SRPA),⁷ these calculations still conform to the simplified concept of quasielastic scattering in which a single nucleon is ejected from the nucleus.

Finally, at the largest momentum transfers for which separated response functions are available, the longitudinal response for medium-sized nuclei is significantly smaller in both overall size and in integrated area than is predicted by simple models of quasielastic (e,e') and is in apparent violation of the Coulomb sum rule.⁸ This has led to a considerable amount of speculation as to the physical source of this suppression. In addition to the possible need for a better description of the many-body dynamics of this process, it has been suggested that the suppression may be due to modification of the nucleon size in the nuclear medium,⁹ quark clustering effects¹⁰ or the result of relativistic dynamics.¹¹⁻¹⁵ Clearly, before appealing to these more exotic suggestions, it is necessary to reconsider the basic assumptions of simple models of quasielastic scattering and to seriously address the many-body nature of the reaction. The major theoretical challenge is to explain the origin of the relative suppression of the longitudinal response while retaining the agreement with the observed transverse response displayed

by simple models.

The basic assumption that the quasielastic (e, e') reaction can be treated solely as the result of the ejection of a single nucleon from the nucleus is highly questionable. Given the size of the energy transfers to the nucleus by the scattering electron which are typical for quasielastic scattering at momentum transfers of several hundred MeV/c, it is clear that many final state channels involving the ejection of multiple nucleons or clusters of nucleons are open. Indeed, in any treatment of the exclusive process ($e, e'N$), which is supposed to dominate the inclusive cross section, it is necessary to allow for a substantial loss of flux to more complicated final states. This is done, for example, by using a nonhermitean optical potential in a distorted wave impulse approximation (DWIA) analysis of this process. Clearly, once this loss of flux is taken into account, simple integration of the exclusive process over missing energy and momentum will seriously underestimate the size of the inclusive response. The inclusive response must include contributions from all open final-state channels.

Several approaches to the final state interactions have been proposed which revolve around a simplified treatment of the final state. The naive argument is that the final state interaction can have no net effect on the total flux to all channels (the Coulomb sum rule) so that the details of the final state interaction can have no appreciable effect on the inclusive quasielastic response. This philosophy has resulted in calculations where the final state interaction has simply been ignored by using the plane wave impulse approximation (PWIA) or where the final state interaction has been included by means of a hermitean potential which may or may not be energy independent.¹⁶ For simplicity, we will refer to them as shell model calculations. Unfortunately, these approaches do not adequately deal with the fact that, although the final state interaction must conserve the total flux, it will redistribute strength as a function of energy and momentum transfer due to differences in the coupling to the available phase space. From a theoretical standpoint these shell model approaches are also unsatisfactory because the hermitean potential, whether it be an energy-independent mean-field potential or the hermitean part of a phenomenological optical potential, is not representative of a many-body treatment of the problem which properly includes the more complicated final state channels. It is then difficult to determine the actual physical content of the calculations and to extend them to a more realistic treatment of quasielastic scattering.

A physically acceptable starting point is to employ a fully realistic complex optical potential such as those which arise from phenomenological analysis of elastic proton scattering or from associated theoretical analyses based on g -matrix or multiple scattering theories. The Green's function approach of Ref. 17 offers a satisfactory way to do this. In this approach, the relationship between forward virtual Compton scattering and inclusive electron scattering is used to construct a one-body approximation to quasielastic electron scattering. Although in Ref. 17 this approximation is motivated by arguments based in multiple scattering theory, the Green's function approach can be derived using standard projection techniques, as is done below. Consequently, the physical content of this approach can be clearly identified. It is essentially a doorway model where a single nucleon initially absorbs the virtual photon, but can couple to more complicated final channels by means of a final state interaction. The reactive content of the nonhermitean part of the optical potential is used to describe the many-body nature of the final state interaction. Being well defined, this model is also extensible, allowing for the calculation of additional many-body corrections which are necessary to remove some of the dynamical inconsistencies inherent in optical model treatments of such processes. By making connection to the optical model, it is possible to constrain the final state interaction by means of elastic nucleon-nucleus scattering, and to take advantage of the considerable body of work on the derivation and properties of microscopic optical potentials.¹⁸⁻³¹ It should also be mentioned that a similar philosophy is the motivation for the extension of the standard RPA to the SRPA which includes multiple-nucleon knockout by calculating all particle lines in the continuum using an optical potential.⁷ Indeed, at large momentum transfers where the effect of long range correlations is negligible the SRPA and the optical model Green's function approach should converge provided that the dynamical input is comparable.

The objective of this paper is to provide a comprehensive study of the role of final state interactions in inclusive quasielastic electron scattering. This study is done in the context of an optical model Green's function approach. A detailed derivation of this approach is presented in Section II in order to clearly identify its physical content and to clarify its limitations. The extension of this derivation to allow for complete antisymmetrization of the theory is presented in the appendix. The incorporation of relativistic dynamics is also described in Section II and is

done in obvious parallel to elastic proton scattering.^{23,26} The computational structure of the relativistic dynamical calculation is sketched in Section III. Numerical results are presented in Section IV for both nonrelativistic and relativistic dynamics. A variety of nonrelativistic optical potentials are used, including theoretical impulse approximation (IA) potentials,²² semi-theoretical local density approximation (LDA) potentials^{18,21} and purely phenomenological potentials.²⁰

Relativistic optical potentials employed span a similar range of models.^{23,27,32} Representative results from an extensive set of calculations are presented. Using these potentials, a number of theoretical experiments are also performed to isolate the importance of various physical processes. Among the results presented are characterizations of the importance of relativistic dynamics, specific virtual pair contributions, off-shell final state processes, and energy-dependent and nonhermitean effects. Section V contains a summary of the results and inferences which may be drawn from our studies.

II. Formalism

In the one photon exchange approximation the (e, e') quasielastic differential cross section in the lab frame can be expressed in the terms of the longitudinal and transverse response functions as:³³

$$\frac{d\sigma}{d\Omega_{k'} d\epsilon_{k'}} = \left(\frac{d\sigma}{d\Omega_{k'}}\right)_{\text{Mott}} \left[\frac{q^4}{q^4} R_L(\vec{q}, \omega) + \left[\tan^2 \frac{\theta}{2} - \frac{1}{2} \frac{q^2}{q^2} \right] R_T(\vec{q}, \omega) \right], \quad (1)$$

where the electron mass is neglected in the extreme relativistic limit assumed here. The Mott differential cross section is that obtained from the scattering of electrons from a point charge. The initial and final four-momenta of the incident electron are k and k' , respectively. The initial bound state and final asymptotic four-momenta of the ejected nucleon will be denoted by p and p' , respectively. The four-momentum transfer carried by the virtual photon is denoted by q , where $q=k-k'$. The space-time coordinates, metric and Dirac algebra follow the notation of Bjorken and Drell.³⁴

The longitudinal and transverse response functions are expressed in terms of the nuclear tensor, which involves the matrix elements of the virtual photon's interaction with the nuclear electromagnetic current:

$$\begin{aligned}
R_L(\vec{q}, \omega) &= W^{00}(\vec{q}, \omega), \text{ and} \\
R_T(\vec{q}, \omega) &= W^{11}(\vec{q}, \omega) + W^{22}(\vec{q}, \omega),
\end{aligned}
\tag{2}$$

where,

$$W^{\mu\nu}(\vec{q}, \omega) = \overline{\sum_i} \left\langle i \left| \hat{J}^{\mu\dagger}(\mathbf{q}) \right| f \right\rangle \left\langle f \left| \hat{J}^{\nu}(\mathbf{q}) \right| i \right\rangle \delta(E_f - E_i + \omega). \tag{3}$$

The initial target state is described by i and f is a particular many-body final nuclear state. $\hat{J}^{\mu}(\mathbf{q})$ is the nuclear electromagnetic current operator, $\hat{J}^{\mu\dagger}(\mathbf{q})$ is the appropriate (Schrödinger or Dirac) adjoint and $\langle f|$ is the corresponding adjoint of $|f\rangle$. Here $\overline{\sum}$ represents an average over initial states. For the quasielastic of interest in this paper it is convenient to suppress the contribution of the discrete states of the set $|f\rangle$ of (3) and to focus on the scattering states, $|f\rangle = |s\rangle$. The nuclear response tensor $W^{\mu\mu}$ can then be written in terms of the forward virtual Compton amplitude $T^{\mu\mu}$, i.e., the elastic scattering of virtual photons from bound nucleons,

$$W^{\mu\mu} = -\frac{1}{\pi} \text{Im } T^{\mu\mu}, \tag{4}$$

where the virtual Compton amplitude is:

$$T^{\mu\nu} = \overline{\sum_i} \left\langle i \left| \hat{J}^{\mu\dagger}(\mathbf{q}) \hat{G}(\omega + E_i) \hat{J}^{\nu}(\mathbf{q}) \right| i \right\rangle, \tag{5}$$

and \hat{G} is the full many-body propagator of the complicated A -body nuclear system (where ' A ' is the atomic number of the target nucleus). Treating the many-body scattering states explicitly, and separately from the bound states, in this manner leads to a continuum doorway approach to the scattering state contribution. Of course at lower energies the discrete state contribution to $W^{\mu\mu}$ must be included by hand. To obtain the response functions an approximation method is introduced to treat the virtual Compton amplitude.

II.A Reduction Formalism

The nuclear response tensor as expressed in (3) or in (4) and (5) is an exceedingly complicated object which defies current computational methods. It is therefore necessary to reduce the complexity of the problem to a tractable computational form. The three basic ingredients which appear in (3), the

initial state, the final states, and the current operator which connects them, are intimately related in any theory. A given Hamiltonian specifies both the initial target wave function $|i\rangle$ and the wave functions $|\psi_f\rangle$ of all of the final nuclear states, as well as which of the latter contribute to (3) for given ω . The current operator is itself a complicated many-body operator whose exact nature depends upon the degrees of freedom described by the wave functions $|i\rangle$ and $|f\rangle$. Generally, the more the number of degrees of freedom suppressed in the wave functions, the more complicated the operator \hat{J}^ν . This is true whether the suppressed degrees of freedom are of the fundamental meson-theoretic type or are due solely to reductions of the (A-body) nuclear many-body problem and its many degrees of freedom.

The most difficult conceptual problem in dealing with (3) is determining a realistic procedure for handling the continuum of scattering final states with their complex many-nucleon knockout character. Simplifications of \hat{J}^ν and $|i\rangle$ introduced to facilitate analysis of the final state continuum in this subsection will be addressed in their own right in Section II.B. Suppose the current operator \hat{J}^ν is so simple that it directly couples the initial target state $|i\rangle$ only to those scattering states which correspond to one-nucleon knockout, that is only to the space spanned by a plane-wave nucleon and an (A-1)-body residual nuclear eigenstate. Denoting these channels by α_i , the associated eigenstates of the (A-1)-body Hamiltonian H_{α_i} by $|\phi_{\alpha_i}\rangle$, defining projectors onto the subspaces in the standard way

$$P_{\alpha_i} = |\phi_{\alpha_i}\rangle\langle\phi_{\alpha_i}| \quad , \quad (6a)$$

and defining the projector onto the full one-nucleon knockout space

$$\Pi = \sum_{\alpha_i} P_{\alpha_i} \quad , \quad (6b)$$

where the sum in (6b) is taken in the sense of a union. Equation (5) becomes

$$W^{\nu\nu} = -\frac{1}{\pi} \text{Im} \sum_i \langle i | \hat{J}^{\nu\dagger}(q) \Pi \hat{G} \Pi \hat{J}^\nu(q) | i \rangle \quad . \quad (7)$$

The special case where $|i\rangle$ is just a single Slater determinant is useful to keep in mind as a simple, concrete example. In that case the α_i just refer to the set of (A-1)-body residual nuclear states ($|\phi_{\alpha_i}\rangle$) that can be formed from the target by removing one nucleon. Except for the azimuthal degeneracies,

these are just the few occupied subshells in number. Noting that a ground state component of Π is immaterial in (7) since $\text{Im } \hat{G}$ contains no such component, and ignoring any nonorthogonality overcompleteness corrections, the operators Π in (7) may be replaced by the literal sum in (6b). A further approximation,

$$\Pi \hat{G} \Pi \approx \sum_{\alpha_i} P_{\alpha_i} \hat{G} P_{\alpha_i} \quad , \quad (8)$$

is introduced so that (7) becomes

$$W^{\nu\nu} = -\frac{1}{\pi} \text{Im} \sum_i \sum_{\alpha_i} \langle i | \hat{J}^{\nu\dagger}(q) P_{\alpha_i} \hat{G} P_{\alpha_i} \hat{J}^{\nu}(q) | i \rangle \quad . \quad (9)$$

Equation (8) is discussed in more detail in the next subsection. In writing (7-9) the Pauli requirement that only properly antisymmetrized states contribute to the spectral form of \hat{G} (See Appendix A) has not been made explicit. The reason for this is that in proceeding further it is desirable to work overtly with a distinguishable ejectile so as not to needlessly obscure essential points. Although there are some interesting theoretical points associated with the fully antisymmetrized treatment, which is presented in Appendix A, all of our main results, namely (16)-(19), remain unchanged. It is now noted that

$$P_{\alpha_i} \hat{G} P_{\alpha_i} = G_{\text{opt}}^{\alpha_i} \quad (10)$$

where $G_{\text{opt}}^{\alpha_i}$ is the α_i -channel one-body optical model Greens function as it is usually defined,^{19,28-30} with optical potential $V_{\text{opt}}^{\alpha_i}$. This result follows immediately from the combination of the resolvent identity

$$\hat{G} = G_{\alpha_i} + G_{\alpha_i} V^{\alpha_i} \hat{G} \quad (11)$$

(right and left projected by P_{α_i}) and the definition of the optical potential

U_{α_i} in terms of the α_i -channel elastic T-matrix T^{α_i} :

$$T^{\alpha_i} = U^{\alpha_i} + U^{\alpha_i} P_{\alpha_i} G_{\alpha_i} T^{\alpha_i} \quad , \quad (12)$$

where

$$T^{\alpha_i} = V^{\alpha_i} \hat{G} G_{\alpha_i}^{-1}, \quad (13)$$

$$V_{\text{opt}}^{\alpha_i} = P_{\alpha_i} U^{\alpha_i} P_{\alpha_i}, \quad (14)$$

and $G_{\alpha_i} = (E - H_{\alpha_i} + i0)^{-1}$ is the α_i -channel free propagator (for the noninteracting nucleon/residual-nuclear system). As a final approximation we take

$$V_{\text{opt}}^{\alpha_i} \approx V_{\text{opt}} \quad (15)$$

where V_{opt} is a specific one-body optical potential, for example, the one associated with the initial target nucleus. Equation (9) now takes the form

$$W^{\nu\nu} \cong -\frac{1}{\pi} \text{Im} \left\{ \bar{\sum}_I \sum_{\alpha_i} \langle i | \hat{J}^{\nu\dagger}(q) P_{\alpha_i} G_{\text{opt}} P_{\alpha_i} \hat{J}^{\nu}(q) | i \rangle \right\}, \quad (16a)$$

$$\cong -\frac{1}{\pi} \text{Im} \left\{ \bar{\sum}_I \sum_{\alpha_i} \langle i | \hat{J}^{\nu\dagger}(q) | \phi_{\alpha_i} \rangle G_{\text{opt}} \langle \phi_{\alpha_i} | \hat{J}^{\nu}(q) | i \rangle \right\}. \quad (16b)$$

Finally, in momentum-space it is convenient to employ a nonspectral form for the optical model Greens function G_{opt} and rewrite (16b) in the form

$$W^{\nu\nu} \cong -\frac{1}{\pi} \text{Im} \left\{ \bar{\sum}_I \sum_{\alpha_i} \langle i | \hat{J}^{\nu\dagger}(q) | \phi_{\alpha_i} \rangle \left(g_0 + g_0 T_{\text{opt}} g_0 \right) \langle \phi_{\alpha_i} | \hat{J}^{\nu}(q) | i \rangle \right\} \quad (16c)$$

where g_0 is the free one-body Greens function and T_{opt} is the optical model T-matrix. Exactly the same equations, (16), are obtained from the fully antisymmetrized development [See Appendix A]. Equation (16c) is of the form actually employed in our numerical work as is discussed in Section III. With the addition of not-too-complicated models for $\hat{J}^{\nu}(q)$, and for the ground and excited wave functions $|i\rangle$ and $|\phi_{\alpha_i}\rangle$, (16) is pragmatically calculable,

requiring as further input only the off-shell T-matrix T_{opt} . Better yet, (16) reduce the sum over the complicated many-body scattering final states to a form which exhibits great conceptual clarity. Using (10) and (15) and the spectral decomposition of the full Greens function, (16) can be rewritten as

$$W^{\nu\nu} \cong \bar{\sum}_I \sum_{\alpha_i} \langle i | \hat{J}^{\nu\dagger}(q) P_{\alpha_i} \left[\sum_S |\psi_S\rangle \delta(\omega + E_i - E_S) \langle \psi_S | \right] P_{\alpha_i} \hat{J}^{\nu}(q) | i \rangle \quad (17a)$$

manifesting the treatment of the scattering states $|\psi_S\rangle$. Let $|\psi_S\rangle$ denote a final state of arbitrary complexity, say for example it is a state which asymptotically corresponds to five-nucleon knockout. In the vicinity of the residual nucleus, $|\psi_S\rangle$ consists of a superposition of many configurations of all asymptotic characters, including a Π -space component, $\sum_{\alpha_i} \langle \phi_{\alpha_i} | \psi_S \rangle | \phi_{\alpha_i} \rangle$.

It is this latter part of $|\psi_S\rangle$ which in (17) couples directly to the ground state through the current operator. More generally,

$$W^{\nu\nu} \cong \sum_I \sum_{\alpha_i} \langle i | \hat{J}^{\nu\dagger}(q) | \phi_{\alpha_i} \rangle \left[\sum_S \langle \phi_{\alpha_i} | \psi_S \rangle \delta(\omega + E_i - E_S) \langle \phi_{\alpha_i} | \psi_S \rangle \right] \langle \phi_{\alpha_i} | \hat{J}^{\nu}(q) | i \rangle \quad (17b)$$

Thus, the set of A-body states which comprise the P_{α_i} serve as a continuum doorway to channels of arbitrary complexity. Such channels are then incorporated, albeit approximately, in the formalism of (16).³⁵ Equation (16c), which was first exploited in Ref. 17, forms the basis for the analysis in this paper. It goes far beyond simple plane-wave or real potential models in providing a clear conceptual treatment of complex many-body reaction channels. It will become clear that it also provides for a straightforward set of immediate correction terms.

To see exactly how (16) extends the analysis of inclusive quasielastic (e,e') beyond simple integrations over the one-nucleon knockout space, it is noted that the unitarity relation satisfied by a generic one-body Greens function, g, with (possibly) nonhermitean optical potential V_{opt} is ($\Delta A \equiv A - A^\dagger$)

$$\Delta g = (1 + V_{opt} g)^\dagger \Delta g_0 (1 + V_{opt} g) + g^\dagger \Delta V_{opt} g \quad , \quad (18a)$$

$$= -2\pi i (1 + V_{opt} g)^\dagger \delta(E_i + \omega - h_0) (1 + V_{opt} g) + g^\dagger \Delta V_{opt} g \quad , \quad (18b)$$

where h_0 is the free one-body Hamiltonian and where in writing (18b) the parametric energy, z, of (18a) is taken to be $z = E_i + \omega$. The operator $(1 + gV_{opt})$ is just the familiar Möller operator which, when operating on a plane-wave state of the same energy, produces the corresponding (outgoing scattered wave) distorted wave. Thus, with $|\chi_{\vec{k}}\rangle$ denoting a distorted wave of asymptotic momentum \vec{k} and incoming scattered wave boundary conditions,³⁶

$$\Delta g = -2\pi i \int d^3k |\chi_k\rangle \delta(E_i + \omega - E_k) \langle \chi_k | + g^\dagger \Delta V_{\text{opt}} g \quad (18c)$$

Comparing (18) with (16) for inclusive quasielastic scattering, a plane-wave integration within the one-body knockout space corresponds to keeping just the Δg_0 part of the first term of (18), while using only the real part of V_{opt} in such a calculation corresponds to dropping the last term of (18) entirely and using only $\text{Re} [V_{\text{opt}}]$ in the first term of (18). The combination of (16) and (18) thus makes evident the additional physics contained in (16) as opposed to calculations which consider only the one-body knockout space of $(e, e'N)$. Similarly, (18) makes clear the crucial correction contained in (16), specifically the second term of (18), which goes far beyond a simple integration over the one-body knockout space in the context of a nonhermitean optical model.

Finally, because (13) for T^{α_i} is Hermitean analytic ($T^{\alpha_i}(z^\dagger) = T^{\alpha_i}(z)^\dagger$, where z is the (complex) parametric energy] and because the structure of (12) passes this property on to U^{α_i} , $V_{\text{opt}}(z)$ is Hermitean analytic. Thus the one-body optical potential V_{opt} satisfies the once-subtracted dispersion relation (E real)

$$\text{Re } V_{\text{opt}}(E) = \text{Re } V_{\text{opt}}(0) + \frac{E}{\pi} \mathcal{P} \int \frac{\text{Im } V_{\text{opt}}(E')}{E'(E'-E)} dE' \quad (19)$$

where it has been assumed that $V_{\text{opt}}(z)$ falls off fast enough as $|z| \rightarrow \infty$ and that there are no singularities of $V_{\text{opt}}(z)$ other than the cut along the positive real axis. The significance of (19) in regard to practical calculations and the Coulomb sum rule is discussed in the next subsection.

II.B Approximations, Limitations, and Corrections

Although the approach of Ref. 17 provides an advantageous basis on which to construct a detailed treatment of the inclusive quasielastic (e, e') reaction, several demanding assumptions have already been made in obtaining (16). These assumptions need to be more clearly stated in the form of approximations and, in addition, several more approximations are required to reduce the problem to the practical calculation described in detail in Section III. Here, the approximation scheme, the limitations of the approach, and the

leading corrections to it are clarified.

It is convenient to discuss each approximation in turn, so the sequence of approximations is listed: [1] The current operator only couples the target ground state to those scattering states which lie in the one-body knockout space, [2] Partial decoupling of the one-body knockout channels (Equation (8)), [3] A common optical potential for all α_i (Equation (15)), [4] Practical approximations for the formally exact operator V_{opt} , [5] Full antisymmetrization and analytic properties versus practical approximations to V_{opt} , [6] Practical approximations to the true many-body bound states $|i\rangle$ and $|\phi_{\alpha_i}\rangle$. Consider each of these six items in turn:

[1] This assumption is the key ingredient of the whole approach. Starting from an elementary current operator in a theory without (acknowledged) suppressed degrees of freedom, one begins with a simple form consisting of a contributing current from each elementary electromagnetically coupled particle. Upon suppressing some of these degrees of freedom, i.e., the explicit appearance of certain final states in the wave functions, a more complicated effective current operator results. In general, this effective current operator will have two- and many-body components. The standard example of this is, of course, the suppression of mesonic and virtual pair degrees of freedom and the resultant effective meson exchange current operators. Similarly, the suppression of purely many-fermion (A-body) degrees of freedom in truncated bound state, one-body optical model, RPA, or coupled-channel theories also implies more complicated effective current operators. The degrees of freedom suppressed in the wave functions are embedded in the effective current operator.

In this paper, all results are calculated on the basis of the usual form of the Dirac free-nucleon current operator. Thus, the free nonrelativistic current and some pair current effects are included. The use of such a free current operator is justified on the basis of simplicity and as a starting point only. It breaks gauge invariance, the current is not conserved, and it is not physically consistent with the wave functions employed. Estimates indicate that ambiguities introduced from this source are at least nonnegligible.³⁷ A firmer basis is needed and corrections must be carefully considered.

There already exists a large literature concerning meson exchange current corrections to approaches such as that employed here.³⁸ For longitudinal response functions these are usually small, due to Siegert's theorem.³⁹ For

the transverse currents these corrections also tend to be small in the region where the one-body current maintains appreciable strength, but can be appreciable in a relative sense once the one-body contribution has fallen off, for example at large q .³⁸ At any rate, the technology for treating such corrections is well developed and can be easily included in the present context. This should prove physically interesting in appropriate regions of four-momentum transfer such as in the dip region between the transverse response and the delta resonance peak. Effective current operator components which result from truncations of many-body scattering and bound state wave functions are not so well documented. Two-body currents resulting from truncated nuclear bound state wave functions are readily accessible, while the analysis of currents implied by optical model truncations of the continuum scattering states is not so readily conceived.

Within this background, assumption [1] can be characterized as follows. For the one-body part of the current operator it is a very reasonable approximation. For two-body and higher-order currents this approximation is not likely to be so reliable, since the current operator can then couple directly to N -nucleon knockout, where $N \geq 2$, even in the case of a single Slater determinant for the target ground state. Thus, the one-body free current operator and one-body correction terms to it should reasonably be expected to be well-treated within the context of (16), at least so long as the $|\phi_{\alpha_i}\rangle$ are well described as a superposition of one-hole states built upon the target ground state (so that the one-hole strength remains concentrated in Π). Two- and many-body meson exchange corrections to the current operator may not be so well represented by (16), but these are small to begin with, so defects are expected to be a correction to a small correction, unless of course one is focusing on the small corrections. Bound state many-body corrections to the effective current operator can be investigated more directly by simply employing more sophisticated bound state wave functions. This should not be affected by assumption [1] except to the extent that the assumed concentration of the one-hole strength in Π is further compromised. Finally, two- and many-body current operator corrections from the optical model truncation are the most problematic elements. To the extent that they turn out to be small, they may be subsumed into the characterization of the exchange currents. However, because of their intrinsic many-body character, they may be more difficult to handle. This issue needs further attention.

[2] Equation (8) is not required to arrive at a doorway model of the

general type of (16), but is only needed to reduce the problem from coupled channel to one-body optical model form. Equation (8) effectively requires only that there be no interference among different doorway channels. This will be a good approximation so long as no "important" final state $|s\rangle$ has appreciable components of more than one doorway state.

Consider first the case of the one-body part of the current operator. From assumption [1], it is assumed that photo-ejection starts the system in a particular state in the doorway space. If this state asymptotically ends up in a one body knockout final state, it is very likely that this will be the same particular doorway state, unless there are strongly coupled collective states. Because the states $|\phi_{\alpha_i}\rangle$ are eigenstates of the Hamiltonian H_{α_i} , they both are orthogonal and specify the final asymptotic configuration of the system when it ends up in the Π -space. Thus, under the stated condition, it is unlikely that such a final state will have an appreciable doorway component other than that which it ends up in. Corrections to this approximation are of order $(1/A)$ and are of the type typically neglected in first order in optical model theories.^{23,30,31} Note that this approximation does NOT entail a simplified nuclear structure description, but only requires that multiple elastic scattering by the ejectile dominate net inelastic transitions within the Π -space.

For more complicated final states, however, this approximation is not likely to do as well. Consider, for example, two-body knockout processes in our single Slater determinant example. In this case the final state $|s\rangle$ may be reached by photo-ejection to form a particular α_i -channel hole-state, followed by nucleon knockout by the photo-ejectile. Obviously, the resultant two-hole state can be reached in two ways, starting with two different α_i channels. It is then evident that interference effects among the α_i channels will generally be important, since $|s\rangle$ will now have appreciable components of more than one of the $|\phi_{\alpha_i}\rangle$ doorway states. It is of course not surprising that one-body optical model analyses should display some defects in their ability to describe two-body and higher knockout. Thus, for treating contributions from higher-order knockout, a coupled channel optical model treatment may provide for a more reliable analysis. For the effective two-body current the foregoing discussion remains relevant, except that physically one now has the potential for direct photo-ejection of two nucleons. This adds another interfering mechanism which can feed two-nucleon

knockout and would seem to make α_1 -channel interference effects even more cogent for analyzing two-body knockout events. This is somewhat academic, however, unless one relaxes the assumption [1] and extends the analysis beyond (7).

It is clear that at least in some cases, at lower energies or momentum transfers and more generally for exploratory purposes, it will be desirable to avoid (8) and instead employ an overall optical model analysis in conjunction with an explicit coupled-channel description of the Π -space. Of course, a simple Hermitean coupled-channel approach within the Π -space is not physically sufficient in and of itself. Nonhermitean optical potentials are still required to treat the important coupling to suppressed channels. It is then clear that such an extension must contain all of the physical effects of (16), and more. Thus, the importance of a realistic treatment of final state dynamics which follows from our numerical results can only be further enhanced.

[3] The use of a common optical potential for all of the α_i channels is perhaps the best justified of the major approximations. In the absence of strongly coupled collective states, and as long as Π concentrates the one-hole strength, the various $|\phi_{\alpha_i}\rangle$ and $|i\rangle$ differ from each other by effects of order $(1/A)$. In the example of a single Slater determinant, the residual nuclear wave functions $|\phi_{\alpha_i}\rangle$ differ from the initial target wave functions $|i\rangle$ by the absence of a single filled nucleon state and from each other by the single-particle state occupied by one nucleon. Many effects of order $(1/A)$ are characteristically neglected in optical model and distorted wave analyses, both formally and practically. Corrections to such approximations typically show little effect on computed results, except in cases where the first order optical potential is specially limited in effect.

[4] The formally exact operator V_{opt} is a very complicated operator with a complex analytic structure reflecting the numerous many-body energy-dependent channel effects subsumed within U^{α_i} . In addition, all of the complexity associated with the many-body bound states $|\phi_{\alpha_i}\rangle$, through which the P_{α_i} are defined, are present as well. Dealing directly with the full operator V_{opt} is essentially as complicated as solving the original many-body problem itself. Thus it is hardly surprising that this operator must be drastically approximated in computational applications. Consequently, much of the formal

content of V_{opt} employed in the developments of Subsection II.A is either lost or only crudely represented. In fact, except in certain circumstances, to say that this operator is approximated is really overly optimistic since the actual approximations involved are not known. A more realistic view is that the operator is simply truncated in a more or less phenomenological manner.

At low energies where individual many-body channels rapidly open as the energy increases and thresholds are reached, the formal optical potential varies rapidly with energy and has a complicated structure.¹⁹ In this regime no completely satisfactory formal development exists and it is probable that current methods, including phenomenology, fail to do justice to the problem. However, as the energy increases to the intermediate energy regime theoretical treatments become more realistic, especially multiple scattering methods, and approximations are under better control. This is typified by the great similarity between phenomenological and theoretical optical potentials and their predicted on-shell scattering amplitudes. Thus it is in this regime that the treatment of final state interactions is likely to be most adequate.

In this paper, nonrelativistic optical potentials from phenomenology,²⁰ local density approximation,^{18,21} and microscopic multiple scattering theory²² are employed. Relativistic optical potentials are generalizations which are constructed more or less in parallel to the corresponding nonrelativistic approach.²³ At low nucleon energies (≤ 100 MeV), and as a realistically energy-dependent operator, it is probable that only purely phenomenological optical potentials are at all reasonable. At intermediate energies (≥ 100 MeV) phenomenological optical potentials of course still most accurately describe the on-shell nucleon-nucleus T-matrix but the multiple scattering theory is best understood conceptually and as a source of off-shell behavior. Here, the convergence of theory and phenomenology indicates that it is not unreasonable to hope that the various optical models are representative of the nature of the true V_{opt} and that their differences reasonably gauge our uncertainty in this regard.

[5] As noted in assumption [4] much of the analytic structure of V_{opt} is lost when drastic approximations necessitated by current methods are made. It is thus necessary to consider whether there are specific constraints which can and need to be imposed on approximate theoretical or phenomenological optical potentials which are to be employed in inclusive quasielastic electron scattering. The fragile nature of unitarity and dispersion relations, especially in the fully antisymmetrized formalism, is discussed in Appendix A.

Of course, detailed unitarity and dispersion properties of V_{opt} are always violated in approximation schemes. Our concern here is that global unitary and dispersion properties of V_{opt} may be unnecessarily violated as well and that this may unduly prejudice (e,e') quasielastic predictions. For example, in Ref. 17 it was observed that, in a particular model, theoretically predicted quasielastic strength systematically overshoot experimental data. This problem was found to be correlated with apparent Coulomb sum rule violations by the calculation of the order of 5-10%. It was then observed that both problems were apparently rectified by imposing the dispersion relation (19). Reference 17 then remarks that "It is interesting to note that quasielastic electron scattering is apparently sensitive to the analytic structure of the optical potential".

However, it is not entirely clear exactly what the essential physics associated with the imposition of relation (19) actually is. Obviously (19) can be used to prevent accidental and unphysical singularities from appearing in the analytic structure of approximate V_{opt} off the positive real energy axis. Equally as obvious, (19) is too strong. It does not follow from (12) and (14). For example, (19) assumes that there are no discrete pole singularities in V_{opt} along the positive real axis and thus forbids associated resonance structure in the physical scattering amplitude.²⁴ In reality this may be physically important at low energies and it is certainly relevant to Coulomb sum rule saturation. Moreover, it is not clear from what significant underlying physical source the excluded singularity structure is derived. Thus, especially in the case of theoretically derived optical potentials, use of (19) remains problematical. It is not clear, for example, that (19) should be used in energy-dependent analyses for joining theoretical models of V_{opt} to phenomenology in regions where the former breaks down, or whether improved energy-dependent phenomenology is to be preferred. No clear constraint of the type of relation (19) is yet apparent.

One constraint which is apparent, in regard to the intermediate state spectral sum in W^{vv} , is the one-body completeness relation and its essential role in preserving the nonrelativistic Coulomb sum rule. Obviously, nonrelativistic analyses which are greatly at variance with the sum rule can not be seriously compared to experiment. One of the advantages of the optical theory Greens function approach in (16) is its automatic incorporation of the completeness relation in the appropriate limit, as expressed in (17). In fact, for nonhermitean optical potentials, this is the essential function of

the last term of (18). In the actual numerical analysis of (16) a nonspectral form of the optical model Greens functions is employed, wherein (16c) is treated by integrating over the scattering amplitude T_{opt} [See section III]. To the extent that the approximate optical potentials employed are reasonable representatives of the true optical potential, (16) guarantees consistency with the completeness relation. Of course, discrete state contributions at lower energies must be added separately. For example, the calculation does not properly incorporate any bound states in the continuum⁴⁰ which may be present. Such normalizable states can arise, in the presence of nonhermitean potentials, as complex eigenvalues. These states are (bi-) orthogonal to the scattering eigenfunctions, which have real eigenvalues. Thus the continuum bound states are not of the character of resonances, and do not lie in the space spanned by the scattering eigenfunctions. In the event that such states exist for a given optical potential they must be included in the completeness relation in order to span the space. On the other hand, such solutions are unphysical in the present case because the optical potential is supposed to reproduce

$$T_{opt} = P_{\alpha_1} T^{\alpha_1} P_{\alpha_1} , \quad (20)$$

where T^{α_1} is the true many body scattering amplitude, which encompasses no such continuum bound states. Thus, for the present case, realistic optical potentials can reasonably be supposed to have no such states and optical potentials which do produce continuum bound states may best be regarded as being unsuitable.

[6] The true many-body bound states $|i\rangle$ and $|\phi_{\alpha_i}\rangle$ must be approximated in practical calculations. Much of the complexity associated with treating these bound states has been lumped in with the preceding discussion of approximations to V_{opt} . What remains in (16b) and (16c) is the appearance of these states in the current matrix elements on either side of G_{opt} . As discussed in assumption [1] truncations of these bound state wave functions result in many-body corrections to the effective current operator sandwiched between them. These higher-order current effects can be investigated by either constructing the correction currents perturbatively or, perhaps more easily, by employing progressively more sophisticated structure models. Unfortunately, no internally consistent approximation scheme for treating the combination of the current operator and the bound states which appear in (16c)

is yet available. This merits further study.

Perhaps the most important role of the nuclear structure is in determining the validity of the key assumption of our whole treatment, namely, [1]. Only if the one-hole strength is concentrated in the Π -space is this assumption justified. Moreover, the degree to which this assumption is broken in more sophisticated nuclear structure models can determine an overall multiplicative factor in the calculated current matrix elements of the one-body current, as well as the nature of correction terms which must be considered in this regard.

Although the various approximations above are obviously both extensive and demanding, it is also clear that (16) forms a very firm basis for a realistic theoretical development. It is conceptually clear in formal content and approximations, while going well beyond previous approaches. The main sequence of approximations seems very well justified in a "first-order" sense. Many corrections and their characters are well-circumscribed. Areas where further work is needed are clearly indicated.

IIC. Relativistic Extension

The preceding subsections contain a full formal development for inclusive quasielastic electron scattering within the context of the nonrelativistic Schrödinger equation. There is no corresponding development for the relativistic dynamical extension. Although relativistic field theory provides a complete formal development in principle, it has not yet yielded a sound development at the level of practical feasibility. This is mainly because of the complexity of the diagrammatics and the associated renormalization program, which so far has made impossible the clear determination of leading relativistic corrections, even for few fermion systems. Unambiguous extraction of such corrections from a field theoretic description of an interacting many-body system is beyond the realm of current methods.

Given this circumstance, one must be satisfied with gauging the implications of "leading" relativistic effects of a more or less intuitive nature, without the benefit of a completely consistent means for doing so. In this paper we focus on possible physical effects which may result from a Dirac dynamical description of the bound and ejected nucleons. Basically, this entails a single particle description of the (bound, ejected) nucleon in which the one-body Dirac equation in the presence of a (Hermitian, complex)

potential is obeyed. The Dirac bound state wave functions employed are those of Ref. 32, while the optical model description of the relativistic final state interactions of the ejectile is taken from Ref. 23, 27 and 32, as described in more detail in Section III. The final ingredient needed to specify the relativistic extension of (16c) employed in this paper is a relativistic current operator. The usual form of the free Dirac electromagnetic current operator is used without any nonrelativistic reductions.

This relativistic extension of the formalism of the preceding subsections has at least two main advantages. First, the extension is done in obvious parallel to Dirac dynamical treatments of elastic proton scattering, the physical process which has so far been the primary domain for such relativistic extensions. Second, the momentum-space approach employed in conjunction with the relativistic extension enables one to, among other things, adopt a closely parallel nonrelativistic limit. One does this³⁷ by simply imposing on the relativistic wave functions the requirement that the lower-components of the Dirac spinors be fixed at the appropriate free-particle value for each value of the momentum. This effectively reduces the problem from four- to two-component spinors, i.e., from Dirac-to-Pauli spin space. One can thus break the relativistic momentum-space wave function into two parts, a "nonrelativistic Pauli wave function" multiplied by the matrix which converts the Pauli spinor into the corresponding free Dirac spinor [See, e.g., Ref. 37 for more detail]. This is in the same spirit as nonrelativistic operators are often defined from matrix elements of their relativistic counterparts, namely, by lumping these Pauli-to-Dirac conversion matrices together with the relativistic operator to put the matrix element into a nonrelativistic form. For example, in the present case the Pauli-to-Dirac conversion matrices and the Dirac current operator can be combined, thus formally rewriting the relativistic current matrix element in terms of nonrelativistic (Pauli) wave functions and an associated nonrelativistic current operator. This is in effect what the definition of our nonrelativistic limit does. It is also noted that the reduction from four to two component spinors described above corresponds to eliminating any negative-energy [i.e., antiparticle and pair] degrees of freedom in the wave function; that is, this reduction confines the wave functions to the positive-energy particle sector of the Dirac Hilbert space.

III. Calculations

In this Section the methods used in the practical implementation of the reduced formalism, as developed in the preceding section, are presented in detail. Actual numerical results are discussed in the following section. Because the nonrelativistic case is a straightforward simplification of the relativistic one, the computational structure used for the relativistic calculations is the one explicitly treated.

To calculate the nuclear response, the forward virtual Compton amplitude is expressed using (5) and (16b) as

$$T^{\mu\nu} = \sum_i \sum_{\alpha_1} \langle i | \hat{J}^{\mu\dagger} | \phi_{\alpha_1} \rangle \hat{G}_{\text{opt}}(\omega + E_1) \langle \phi_{\alpha_1} | \hat{J}^\nu | i \rangle . \quad (21)$$

In the numerical evaluation of (21) the usual form of the free Dirac current operator is employed and a variety of optical potentials are investigated as sources for $\hat{G}_{\text{opt}}(\omega + E_1)$. Since the focus is on dynamics in this paper, a simple Slater determinant of one-body nuclear states is employed to represent the target ground state wave function $|i\rangle$. Corrections due to more sophisticated nuclear structure models are not expected to be crucial in the momentum transfer region of interest in this study. Similarly, the one-body knockout states $|\phi_{\alpha_1}\rangle$ are taken to differ from $|i\rangle$ only in the absence of the ejected nucleon so that differences between the target and residual nuclear Hamiltonians are neglected. With these approximations, the one-body nature of \hat{J}^μ is sufficient to reduce (21) to a one-body matrix element, provided one also ignores nonorthogonality terms which arise from the nonzero overlap of distorted waves and single-particle bound state wave functions. Thus, (21) becomes

$$T^{\mu\nu} = \sum_i \langle \overline{i_{(1)}} | \hat{J}_{(1)}^{\mu\dagger} \hat{G}_{\text{opt}}(\omega + E_1) \hat{J}_{(1)}^\nu | i_{(1)} \rangle , \quad (22)$$

where the sum is over the nuclear single-particle states $|i_{(1)}\rangle$ which are occupied in the target, the subscript (1) is used to emphasize the one-body nature of the quantities which appear in (22), the Dirac adjoint state has been made explicit, and the \dagger denotes the Dirac adjoint for the remainder of this section.

This expression for the forward virtual Compton amplitude is given in

momentum space by

$$T^{\mu\nu} = \sum_i \int \frac{d^3\vec{\ell} d^3\vec{p} d^3\vec{p}' d^3\vec{\ell}'}{(2\pi)^{12}} \overline{\langle i_{(1)} | \vec{\ell} \rangle} \langle \vec{\ell} | \hat{J}_{(1)}^{\mu\dagger} | \vec{p} \rangle \langle \vec{p} | \hat{G}_{\text{opt}}(\omega+E_1) | \vec{p}' \rangle \langle \vec{p}' | \hat{J}_{(1)}^{\nu} | \vec{\ell}' \rangle \langle \vec{\ell}' | i_{(1)} \rangle \quad (23)$$

where the matrix elements are

$$\begin{aligned} \langle \vec{\ell} | \hat{J}_{(1)}^{\mu\dagger} | \vec{p} \rangle &= J^{\mu}(-q) (2\pi)^3 \delta^{(3)}(\vec{\ell} - \vec{p} + \vec{q}) \\ \langle \vec{p}' | \hat{J}_{(1)}^{\nu} | \vec{\ell}' \rangle &= J^{\nu}(q) (2\pi)^3 \delta^{(3)}(\vec{\ell}' - \vec{p}' + \vec{q}) \\ \langle \vec{p} | \hat{G}_{\text{opt}}(\omega+E_1) | \vec{p}' \rangle &= (2\pi)^3 G_{\text{opt}}(\vec{p}, \vec{p}'; E) \quad , \quad E = \omega + E_1 \end{aligned} \quad (24)$$

In (24) the bar indicates a Dirac conjugate, $\overline{\langle i | \vec{\ell} \rangle} = \langle \vec{\ell} | i \rangle^{\dagger} \gamma_0$ and $G_{\text{opt}}(p, p'; E)$ is the full one-body optical model Green's function. The forward virtual Compton amplitude is thus

$$T^{\mu\nu} = \sum_i \int \frac{d^3\vec{p} d^3\vec{p}'}{(2\pi)^3} \overline{\langle i | \vec{p} - \vec{q} \rangle} J^{\mu}(-q) G_{\text{opt}}(p, p'; E) J^{\nu}(q) \langle \vec{p}' - \vec{q} | i \rangle . \quad (25)$$

The optical model propagator is then written as:

$$G_{\text{opt}}(p, p'; E) = G_0(p) \delta^{(3)}(\vec{p} - \vec{p}') + G_0(p) T_{\text{opt}}(p, p'; E) G_0(p') , \quad (26)$$

where $G_0(p)$ is the free Dirac propagator and $T_{\text{opt}}(p, p'; E)$ is the fully off-shell Dirac optical model nucleon-nucleus T -matrix. Combining (25) and (26), yields

$$\begin{aligned} T^{\mu\nu} &= \sum_i \int \frac{d^3\vec{p}}{(2\pi)^3} \overline{\langle i | \vec{p} - \vec{q} \rangle} J^{\mu}(-q) G_0(p) J^{\nu}(q) \langle \vec{p} - \vec{q} | i \rangle \\ &+ \sum_i \int \frac{d^3\vec{p} d^3\vec{p}'}{(2\pi)^3} \overline{\langle i | \vec{p} - \vec{q} \rangle} J^{\mu}(-q) G_0(p) T_{\text{opt}}(p, p'; E) G_0(p') J^{\nu}(q) \langle \vec{p}' - \vec{q} | i \rangle . \end{aligned} \quad (27)$$

The first term gives rise to the plane wave approximation, where the ejected nucleon is described by a free Dirac wave function and is not distorted by any nuclear potential. The second term is the modification caused by the final state interactions of the ejected nucleon with the residual nucleus.

To evaluate (27) $G_0(p)$ is expanded into positive- and negative-energy solutions $|\vec{p}, \alpha, \pm\rangle$ of the free Dirac equation for momentum \vec{p}

$$G_0(p) = \frac{1}{\gamma \cdot p - m_N + i\epsilon} \quad (28)$$

$$= \left[\frac{\sum_{\alpha} |\vec{p}, \alpha, +\rangle \langle \vec{p}, \alpha, +|}{E - E_p + i\epsilon} + \frac{\sum_{\alpha} |\vec{p}, \alpha, -\rangle \langle \vec{p}, \alpha, -|}{E + E_p + i\epsilon} \right] ,$$

where $E_p = \sqrt{\vec{p}^2 + m_N^2}$, m_N is the nucleon mass, (+, -) denotes a (positive, negative) energy solution, and α labels the Pauli spin state. Upon inserting (28) into (27) and making use of the following notational assignments:

$$\overline{\langle \vec{p}, \alpha, \pm | T_{\text{opt}}(p, p'; E) | \vec{p}', \beta, \pm \rangle} = T_{\alpha\beta}^{\pm\pm}(p, p') , \quad (29)$$

$$= \chi_{\alpha}^{\dagger} T^{\pm\pm}(p, p') \chi_{\beta} ,$$

$$\overline{\langle \vec{p}, \alpha, \pm | J^{\mu}(q) | \vec{p}-\vec{q}, i \rangle} = J_{\alpha i}^{\mu}(q, \vec{p}, \pm) , \quad (30)$$

where χ_{α} is a Pauli spinor, the second term of the forward virtual Compton amplitude of (27) becomes:

$$\Delta T^{\mu\nu} \equiv \int_i \int \frac{d^3 p d^3 p'}{(2\pi)^3} \left\{ J_{\alpha i}^{\mu}(q, \vec{p}, +)^* \frac{1}{E - E_p + i\epsilon} T_{\alpha\beta}^{++}(p, p') \frac{1}{E - E_{p'} + i\epsilon} J_{\beta i}^{\nu}(q, \vec{p}', +) \right.$$

$$+ J_{\alpha i}^{\mu}(q, \vec{p}, +)^* \frac{1}{E - E_p + i\epsilon} T_{\alpha\beta}^{+-}(p, p') \frac{1}{E + E_{p'} - i\epsilon} J_{\beta i}^{\nu}(q, \vec{p}', -) \quad (31)$$

$$+ J_{\alpha i}^{\mu}(q, \vec{p}, -)^* \frac{1}{E + E_p - i\epsilon} T_{\alpha\beta}^{-+}(p, p') \frac{1}{E - E_{p'} + i\epsilon} J_{\beta i}^{\nu}(q, \vec{p}', +)$$

$$\left. + J_{\alpha i}^{\mu}(q, \vec{p}, -)^* \frac{1}{E + E_p - i\epsilon} T_{\alpha\beta}^{--}(p, p') \frac{1}{E + E_{p'} - i\epsilon} J_{\beta i}^{\nu}(q, \vec{p}', -) \right\} .$$

The evaluation of (29) - (31) now proceeds as follows. In order to calculate R_L and R_T in a relativistic framework, the nuclear electromagnetic current operator is taken to be the free Dirac single-nucleon current operator

$$J^{\mu}(q) = F_1(q^2) \gamma^{\mu} + i \frac{F_2(q^2)}{2m} \sigma^{\mu\nu} q_{\nu} . \quad (32)$$

with form factors taken from ref. 41 and modified as in ref. 42. The Dirac momentum-space bound state wave functions $\langle \vec{p}-\vec{q}, i \rangle$ of ref. 32 are then used to

compute (30). No nonrelativistic P/m expansion of the current operator is employed.

As is apparent from (29) and (31), T-matrix elements are needed at momenta "p" and "p'" which are off-shell. In fact, it turns out that off-shell structure plays a significant role in determining the quasielastic response functions. The off-shell nucleon-nucleus T-matrix elements needed in (29) are calculated through the use of a relativistic Lippmann-Schwinger-like integral equation as detailed in ref. 22 and 23. The code "WIZARD", modified to accept an assortment of relativistic and nonrelativistic optical potentials and to generate fully off-shell T-matrices, provides the needed T-matrix elements in partial wave form.^{22,23} The partial wave T-matrices are combined with partial wave expansions of the $J_{\beta i}^{\mu}$ [See, e.g. Ref. 37] to facilitate calculation of (31). A number of tests were performed to verify the numerical consistency and accuracy of the calculations, including comparisons with previous^{12,13} results for real Hartree FSI.

As is apparent in (31), quasielastic contributions arise not only from positive-energy, but also from explicit negative-energy t-matrix couplings. In fact, there are two distinct sources of such negative-energy contributions present in (31). Figure 1 shows a diagram of the FSI contribution to the forward virtual Compton amplitude corresponding to (31). An explicit source of negative-energy contributions is manifest in the second, third and fourth terms in (31). These terms involve T^{+-} , T^{-+} and T^{--} and correspond to the physical situation where at least one virtual photon in Fig. 1 directly couples to a negative-energy nucleon channel at its vertex. The second source of negative-energy contributions arises implicitly through the T-matrix element T^{++} in the first term in (31). After the nucleon has been ejected from the nucleus, final state interactions represented by "T" in Figure 1 couple the nucleon to negative-energy channels in intermediate states. In other words, the integral equation which determines T^{++} contains couplings to negative-energy intermediate states through the Dirac optical potential. The practical significance of these two types of negative-energy contributions for the quasielastic response functions is detailed in the next Section.

IV. Results

Representative results of extensive calculations of the longitudinal and transverse response functions for the inclusive quasielastic (e,e') reaction,

within the context of (16c), are presented in Figures 2-16. In this paper we are basically interested in physically observable effects (and their character) which may arise from final state interactions (FSI). To study such FSI effects in detail, nonrelativistic and relativistic dynamic calculations have been performed within the context of a number of models and with the capability of isolating several distinct physical processes. Results are shown for slices through the q - ω plane, as a function of ω for three fixed q values: $q = 410$ MeV/c, $q = 550$ MeV/c, and $q = 700$ MeV/c. Since the point of our study is to explore the physical implications of a variety of theoretical and phenomenological treatments of the FSI, no adjustable parameters are used, either in the microscopic theoretical or in the phenomenological models. Even for the lowest momentum transfer, $q = 410$ MeV/c, the quasielastic peak occurs at $\omega > 100$ MeV, so that microscopic multiple scattering theory should be reasonably applicable, especially at and above the peak. Of course, as ω decreases below 80-100 MeV, the microscopic theory becomes increasingly untenable and phenomenology must be relied upon. Thus the quasielastic calculations associated with microscopic multiple scattering optical potentials should not be taken too seriously for small ω .

For each relativistic and nonrelativistic calculation, the corresponding "on-shell" and plane wave limits are isolated for comparison. The plane wave limit is the result of (16c) when there are no FSI, that is when $T_{opt} \equiv 0$. The calculation which is referred to as "on-shell" incorporates into (16c) only the on-shell part of T_{opt} [See Section III].³⁷ The momentum-space matrix elements of T_{opt} involve initial and final momenta, \vec{p}' and \vec{p} , corresponding to energies generally different from the parametric energy E of $T_{opt}(E)$, which specifies the energy of the asymptotic ejected nucleon. Off-shell kinematics is the general circumstance, since only when all three of these energies coincide is $T_{opt}(E)$ on-shell, (i. e., $E = \sqrt{\vec{p}^2 + m_N^2} = \sqrt{\vec{p}'^2 + m_N^2}$). The distinction between on-shell FSI effects and those which appear exclusively off-shell is important because the former are observable in elastic proton scattering and are thus much more securely known. The off-shell behavior of T_{opt} is typically extrapolated using some theoretical ansatz, such as meson theory. In the present case of quasielastic electron scattering effects which derive from the on-shell part of T_{opt} are on a very solid footing. The purely on-shell calculation is also of interest because the various models which we investigate do not precisely agree in their on-shell predictions for T_{opt} , a defect which should in principle be remedied by minor parametric adjustments

within the models. Comparison of the quasielastic predictions of the various models in conjunction with a comparison of their corresponding on-shell limits then enables one to gauge the degree to which differing quasielastic predictions made by the models reflect their intrinsic dynamical differences rather than just their differing precisions in describing the known on-shell amplitude.

In the nonrelativistic case the quasielastic predictions of phenomenology, impulse approximation and LDA treatments of the FSI are compared. These are then contrasted with corresponding predictions made on the basis of several relativistic models. The relativistic models of the FSI employed include a microscopic impulse approximation optical potential, a global energy-dependent phenomenological parameterization and a (Hermitean) Hartree potential.

In the relativistic dynamical calculations two sources of negative-energy contributions or virtual pair effects are isolated. The explicit source involves direct vertex couplings by T_{opt} to negative-energy states, represented by the last three terms in (31). Turning off these explicit pair effects yields a calculation referred to as NEP (no explicit pair effects). Even if only positive-energy matrix elements of T_{opt} are used, virtual pair effects still derive from the integral equation²³ used to obtain T_{opt} from V_{opt} . If, in addition to neglecting the explicit negative-energy contributions, pair effects are turned-off in the integral equation, a calculation referred to as NP (no pair effects) is obtained. This is a purely positive-energy limit, in the sense that all Dirac sea effects are removed. The capability to perform these distinct calculations allows us to isolate and uncover the exact source of specific pair effects seen in the quasielastic predictions. The NP limit must be used with some care since turning off pair effects in the integral equation for T_{opt} will produce a different on-shell scattering amplitude. Nevertheless, to the extent that the on-shell T_{opt} are not markedly different, the NP limit defines a useful corresponding nonrelativistic limit.

Before discussing individual figures there are several general results which can be inferred globally from the figures. First, in each figure the relativistic plane-wave calculation is shown as a reference curve. The corresponding nonrelativistic calculation is not shown in any of the figures, since the two plane-wave calculations are virtually identical. The input to these calculations differs only in the presence or absence of negative-energy

components in the bound states. As discussed in Section II.C, there is no ambiguity introduced by differing current operators, thus virtual pairs (negative-energy components) in the bound state wave functions are completely negligible as far as quasielastic (e, e') is concerned, at least in areas of the $q-\omega$ plane where the longitudinal and transverse response functions are appreciable.

Second, FSI are never neglectable. In no case is the plane-wave approximation adequate. Similarly, off-shell FSI effects are found always to be qualitatively important. FSI always suppress the peak heights of both response functions considerably and the size of this effect is dynamically dependent as is the relative effect on the transverse and longitudinal response functions. Because of the unitary nature of (16) and (18) and in accord with the nonrelativistic Coulomb sum rule, the strength subtracted from the peaks by the FSI is largely dispersed to the high energy tails of the distribution, broadening it considerably. Thus, the effect of the FSI is mainly to redistribute the quasielastic strength in the $q-\omega$ plane, changing the overall shape of the distribution. The character of the various dynamical calculations with regard to the Coulomb sum rule is discussed in detail elsewhere,⁴³ here it is simply noted that our various results typically saturate the sum rule to within about 10%. Our immediate conclusions are thus: (1) Proper inclusion of FSI is crucial for meaningful comparison of theoretical results with experimental data, (2) The direct physical approach of (16) provides an advantageous framework for analyzing FSI effects in inclusive quasielastic (e, e'), and, in addition, (3) Off-shell FSI effects are invariably important, can never be neglected or approximated away, and show considerable sensitivity to the theoretical model employed.

Finally, the various models differ greatly in the degree of their agreement with the experimental data for the transverse and longitudinal response functions, although several characteristic trends can be discerned, as is discussed later. Nevertheless, the general result is that in no case is simultaneous agreement between theory and experiment for both response functions found. The implications of this failure, and the way it occurs in the various models, is discussed in detail later.

Figures 2a and 2b compare several nonrelativistic calculations at a momentum transfer of 410 MeV/c for R_L and R_T , respectively. The short-dashed curves correspond to an optimally factorized impulse approximation (IA) optical potential²² using Franey-Love N-N amplitudes⁴⁴ and the dot-dashed

lines to an IA optical potential using Franey-Love amplitudes in the local $t(q) \rho(q)$ approximation.¹⁸ The solid curves correspond to a local density approximation (LDA) optical potential constructed using Bonn N-N amplitudes.²¹ The predictions of a nonrelativistic, phenomenological, energy-dependent, Woods-Saxon potential fitted²⁰ to proton scattering data is also displayed in Fig. 2 as the long-dashed curve. In Figs. 2a and 2b there is a dramatic difference between the plane-wave calculation and the others. The FSI greatly reduce the quasielastic peak heights, broaden the distributions, shift the position of the peaks, and enhance the high- and low-energy tails of both response functions.

The two nonrelativistic IA calculations make very similar quasielastic predictions. Apparently, differing IA prescriptions result in little quasielastic (e, e') ambiguity once the input two-body amplitudes are specified. The predictions of the phenomenological optical potential are quite different, being much less suppressed relative to the plane wave limit at the quasielastic peak. This dichotomy is easily understood on the basis of results from elastic proton scattering, where the absorptive potentials predicted by the IA tend to be considerably stronger than those obtained from phenomenology.²⁵ The elastic proton data of course favors the phenomenological potential, however elastic predictions are somewhat insensitive to such differences due to the fact that black-disc scattering dominates and further increases in the "blackness" in the nuclear interior are relatively unimportant. Evidently the quasielastic (e, e') reaction is more sensitive to the character of the absorptive potential. Stronger absorption further depletes the quasielastic strength relative to the plane wave prediction at the quasielastic peak. In view of the unitary nature of (16) the strength drained from the plane wave response by the absorptive potential is then shifted in the $q-\omega$ plane to broaden the distributions and enhance their tails. LDA optical potentials typically display greater similarity to phenomenological potentials than do IA optical potentials. This is due to LDA density corrections which significantly suppress the imaginary potentials^{18,21} and is consistent with the close agreement seen in Fig. 2 for the quasielastic (e, e') predictions made by the LDA and phenomenological optical models.

The nonrelativistic on-shell results, shown in Figures 2c and 2d, are very similar in size and shape, supporting the earlier claim that the on-shell matrix elements of the various T_{opt} are much better constrained. It would be very surprising if this were not the case. In comparison with the full

calculation the on-shell curves are greatly suppressed, emphasizing the importance of off-shell contributions. The large differences observed in the full calculations are not reflected in the on-shell results, indicating that these effects are due to the different off-shell extensions of T_{opt} . Also, the high-energy tails in the full calculations are seen to be solely the result of off-shell contributions, as expected.

In Figure 3 analogous calculations are shown at a momentum transfer of 550 MeV/c. Although these figures show much the same qualitative features as in Fig. 2, the differences among the various calculations are much smaller. The two IA calculations are again very close together, showing almost identical results. The LDA calculation is now much closer to the other calculations than it was at 410 MeV/c. This is consistent with the behavior of LDA modifications to the N-N amplitudes, which fall as the energy increases or as the momentum transfer increases at fixed energy. Figure 3 also suggests that at higher momentum transfer reasonable nonrelativistic FSI may display less variability in their quasielastic (e, e') predictions. Results for the phenomenological potential used in Fig. 2 are not shown here because of the restricted range of validity of this potential.

The nonrelativistic FSI suppress the peak heights (relative to the corresponding plane-wave calculation) of both response functions. In comparing the effect on the two response functions, the suppression of R_T is slightly greater than that for R_L . This is a consistent feature of our calculations that is not at all in agreement with the trend observed in the experimental data. While suppression of the peak height of R_L is needed for agreement with the data, the FSI-induced suppression is too small by a factor of about 2. Moreover, in the case of R_T , little if any suppression is apparently required by the data, while the predictions using realistic FSI imply a suppression of about 20%. However, this latter contradiction need not be taken too seriously since it is evident from the data that much more transverse strength is present in (and below) the dip region above the quasielastic peak, and that this strength is large enough to affect R_T at its peak.⁴⁶ Whatever the source of this additional strength, it is then clear that it can appreciably enhance the quasielastic peak so that appropriate FSI suppressions of R_T will ultimately play an important role in achieving theoretical consistency with the R_T data. In this regard, it is important to emphasize that the transverse anomaly can have absolutely nothing to do with validating, in any sense, a plane-wave treatment for R_T . All of the

transverse quasielastic strength contained in the plane-wave limit is present in the treatment of (16c) of the FSI, by virtue of its unitary character in the P_{α_1} -space as expressed, for example, by (17) and (18). This is also made obvious by writing Δg in (18) in its (biorthogonal) spectral form and noting that the energy integral then just reproduces the one-body plane-wave completeness relation.³⁶ Thus, the effect of the FSI is to redistribute the transverse strength in the q - ω plane by dispersive processes which, physically, must be present. Whatever the additional physical mechanism responsible for the observed enhancement of the transverse quasielastic peak, it must be in addition to the physics contained in the nonrelativistic optical model treatment of the P_{α_1} -space and thus physically has nothing to do with the plane-wave limits. Finally, in contrast to the transverse case, the shape of the longitudinal quasielastic peak appears to be in qualitative agreement with the data. The nonrelativistic FSI systematically overestimate the peak heights of R_L as found in earlier calculations.⁴⁵

In discussing the figures individually it is now convenient to make some global symbolic assignments of curve types. In the following figures the dotted curve denotes the relativistic plane-wave calculation for the relevant value of q . Dot-dashed curves represent the on-shell limit of the calculation depicted as a dashed curve in the same figure, with short or long dashes being used to distinguish between different sets of curves.

Quasielastic predictions made on the basis of two relativistic dynamical descriptions of the FSI are displayed in Figures 4 and 5 at momentum transfers of 410 MeV/c and 550 MeV/c, respectively. In each figure the long-dashed line denotes the prediction based on the global, phenomenological energy-dependent, relativistic optical potential of Ref. 27, while the short-dashed curve denotes the microscopic relativistic IA optical potential of Ref. 23. The former is simply referred to as the "relativistic global" FSI. The corresponding on-shell calculations are also shown and are denoted in accord with the convention described earlier. In both figures and for both FSI the importance of the redistribution of strength caused by the FSI, which reduces the quasifree peak and enhances the tails of the distributions, is again observed. Quantitatively, however, the trends are somewhat different than for the nonrelativistic dynamics. In Figure 4 the suppression of the longitudinal quasifree peak (relative to the plane wave prediction) by the relativistic FSI is about 26% for the global potential and about 38% for the IA potential.

Similarly, the suppression of the transverse response is about 19% for the global potential and about 32% for the IA potential. The same pattern is found at $q=550$ MeV/c in Figure 5, with the peak longitudinal response producing a reduction of about 27% for the global potential and about 32% for the IA optical potential, while the suppression of the transverse response is about 22% for the global potential and about 25% for the IA potential. Thus, in all of the relativistic dynamical calculations the suppression of the longitudinal is slightly greater than the suppression of the transverse quasielastic response. This is opposite to the trend observed for the quasielastic response based upon nonrelativistic dynamics.

The IA predictions for the longitudinal response are now in good agreement with the data at 410 MeV/c and are approaching agreement at 550 MeV/c. The corresponding predictions of the global potential do not fare quite so well, considerably overpredicting the peak strength at both q values. The IA predictions also graphically emphasize that it is the relative R_L-R_T peak size which needs to be understood, not simply a suppression of R_L , because the agreement with R_L is good while R_T is inexplicably large. Too much should not be made of this, however, since the reasons for the difference between the predictions of the relativistic global and IA FSI are not clear. On the other hand, this change of focus, from an apparent suppression of R_L to an apparent enhancement of R_T , receives some support from recent exclusive measurements where an unexplained enhancement of R_T was observed.⁴⁶ The on-shell predictions do not reflect any systematic deviations. The two relativistic potentials yield similar, but not identical on-shell results. At 410 MeV/c Figure 4 reveals that most of the differences between the predictions of the two potentials is due to differing off-shell contributions. The opposite is true at 550 MeV/c in Figure 5 in that the differences appear to be primarily on-shell in nature. This can be attributed to the fact that at higher momentum transfers (and therefore higher ejected nucleon energies) more and more of the strength is near the on-shell limit, as should be expected. Finally, it is noted that there exists a qualitative agreement between the relativistic dynamical predictions and the data, particular for both tails of the longitudinal distribution, and the low-energy tail of the transverse response.

It has already been noted that the nonrelativistic FSI tend to suppress R_T slightly more than R_L (relative to the plane wave approximation), while the relativistic FSI suppress R_L more than R_T . To better observe these relative

suppressions, representative quasielastic predictions of the relativistic and nonrelativistic dynamical models are explicitly compared in Figures 6-9. Figs. 6 and 7 compare the predictions made by the relativistic global FSI to those of the nonrelativistic LDA optical potential at 410 MeV/c and 550 MeV/c, respectively. The nonrelativistic LDA calculation was seen in Figs. 2 and 3 to be representative of nonrelativistic phenomenology at 410 MeV/c and of generic nonrelativistic results at 550 MeV/c. Figures 8 and 9 compare the $|\vec{q}| = 410$ and 550 MeV/c quasielastic predictions made by the microscopic relativistic and nonrelativistic IA optical potentials of Ref. 22 and 23. The corresponding on-shell limits are shown for all of these cases. Although the on-shell predictions shown in the comparisons of Figs. 6-9 do show some differences in detail, it is clear that this is not the effect of primary importance. In all four figures, at the quasielastic peak, the additional suppression of the longitudinal response due to relativistic dynamics is much larger than the additional relativistic suppression found for the transverse response. In fact, the relativistic suppression of R_L is about 20% whereas the corresponding suppression of R_T is on the order of 10% or less. Purely nonrelativistic FSI dramatically suppress R_T relative to R_L at the quasifree peak, while the converse is true with added relativistic FSI dynamics. Thus, relativistically, the transverse response function is reduced slightly, while the longitudinal response is suppressed significantly towards the data. If the relativistic Global FSI are compared directly with the nonrelativistic IA predictions the longitudinal response is suppressed by 3% at $|\vec{q}| = 410$ MeV/c and 11% at $|\vec{q}| = 550$ MeV/c, while R_T is enhanced by 11% at $|\vec{q}| = 410$ MeV/c and suppressed by about 2% at $|\vec{q}| = 550$ MeV/c. In this case the phenomenological evidence is overwhelmingly in favor of including relativistic dynamics. In comparing the on-shell-only results in Figures 6 and 7 there doesn't appear to be any systematic behavior, while in Figures 8 and 9 some of the trends observed in the full calculations can be traced to the on-shell contributions. The on-shell effects are not very large and it is clear that the main effects are due to the off-shell behavior of T_{opt} . The origin of the observed relativistic FSI effects is clarified in the next set of figures.

Physically, the main differences between the relativistic and nonrelativistic calculations are the contributions that arise due to negative-energy channel effects in the relativistic optical potentials and T-matrices. Figures 10-12, for $q = 410$ MeV/c, 550 MeV/c, and 700 MeV/c, respectively, resolve the global relativistic quasielastic predictions into

their component parts. As described earlier, the negative-energy contributions can be ascribed to two categories. The NEP calculation includes virtual pair effects used in the construction of the positive projection of T_{opt} , while excluding explicit negative-energy state couplings by T_{opt} . The full calculations are depicted by the long-dashed line and the corresponding NEP and NP calculations by the solid and short-dashed curves, respectively. Associated on-shell limits follow our standard convention and again the differing on-shell FSI effects are not of essential importance. Because the NP limit is reached by turning off all final state pair effects, it may be regarded as something of a nonrelativistic limit of the global relativistic calculation. In fact, the NP limit of the relativistic IA calculation is the nonrelativistic IA calculation by definition (See ref. 23). If the global NP limits are compared with the nonrelativistic predictions of the preceding set of figures, Figs. 6-9, the off-shell differences between these two "nonrelativistic" calculations account for about 50% of the additional relativistic suppression of R_L seen in Figs. 6-9 and essentially all of the additional suppression of R_T . For R_L turning off only the explicit pair contributions reduces the suppression of the quasielastic peak. Turning off the remaining pair contributions (virtual pairs in intermediate states in the integral equation for T_{opt}), in addition, further reduces the suppression. Thus for R_L both pair contributions suppress the peak quasielastic strength. For R_T the trends are somewhat different, with turning off the explicit pair contributions suppressing the quasifree peak. Turning off the remaining pair contributions then effectively cancels this effect. Thus for R_T explicit pair contributions enhance the quasielastic peak, but this is canceled by the suppressive effect of the remaining pair contributions. The net result is that off-shell effects of a nonrelativistic type account for half of the relativistic suppression of R_L and all of the relativistic suppression of R_T . Manifest pair contributions account for half of the relativistic suppression of R_L , but have little effect on R_T . The net effect seen due to negative-energy contributions is typical of all relativistic potentials examined.

As a side note a very interesting trend is seen in Figures 10, 11 and 12, involving the off-shell contributions. As the momentum transfer $|\vec{q}|$ is increased, the predicted response functions are increasingly well-represented by their on-shell limit. This is not a surprising result and in Figures 12a and 12b the on-shell-only curves are almost the same size as the full curves. However, the large high-energy tail and shape modifications due to off-shell

effects remain even at 700 MeV/c. Within the nuclear medium the final state interactions shift the ejected nucleon off-shell, but as the momentum transfer increases, the ejected nucleon becomes relatively less affected by medium effects near the quasielastic peak. However, the tails always depend upon momentum-transfer sharing with the FSI so that even at $|\vec{q}| = 700$ MeV/c there is still a significant off-shell effect.

Figures 13-16 investigate the effect of nonhermitean FSI on the quasielastic response functions. Figures 13-15 compare, at $q = 410$ MeV/c, 550 MeV/c, and 700 MeV/c, respectively, the quasielastic predictions associated with the global relativistic optical potential, (long-dash) and those obtained from a Hermitean relativistic Hartree potential, (solid).³² Also shown in these figures is a comparison of the quasielastic predictions of the NP "nonrelativistic" limit for both the Global (short-dash) and Hartree (dot-dash) FSI. As is to be expected, because the Greens function formalism preserves the completeness relation on the one-body space, no dramatic reduction in overall quasielastic strength results from nonhermitean optical potentials. Rather, the effect of the nonhermiticity is, and can only be, to provide a somewhat different dispersive mechanism through which to redistribute the quasielastic strength. This is discussed in more detail relative to the Coulomb sum rule elsewhere.⁴³ As is evident in Figs. 13-15, for the peak of the longitudinal response, where the relativistic effects are larger than for the transverse case, the nonhermitean effects are much smaller than the differences between relativistic and NP "nonrelativistic" predictions. For the transverse response, however, nonhermitean effects are somewhat larger at the quasielastic peak. It is clear from these figures that there is a systematic difference in shape between the energy-dependent, nonhermitean, global optical potential and the energy-independent, Hermitean, Hartree potential for both relativistic and nonrelativistic dynamics. The response functions for the Hartree potential are noticeably broader than the corresponding response functions for the global potential. Since the integrated strength should be roughly the same for Hermitean and nonhermitean potentials, the response functions for the global potential have a much larger high energy tail than those for the Hartree potentials, which compensates for the relatively narrow quasielastic peak. These differences in shape become more pronounced with increasing momentum transfer.

In comparing the shapes of the quasielastic peaks calculated with the energy-independent Hartree and the global energy-dependent phenomenology, it

is apparent that the energy dependence of the potentials is important. The energy dependence is related to the analytic structure of the optical potential, where the real and imaginary parts are connected through a dispersion relation. Energy dependence also arises from the nonlocal structure of the optical potential. It is apparent that the quasielastic response functions calculated in the optical model approach are sensitive to the energy dependence of the optical potential.^{17,43}

Finally, the full relativistic global calculation (dashed-line) is compared in Fig. 16 to predictions from an otherwise identical calculation in which the nonhermitean part of the Dirac global optical potential is turned off (solid line). Here, as might be expected, the observed effects of the nonhermiticity on the quasielastic response are more distinctive, with the quasifree peaks showing an appreciable suppression due to nonhermitean FSI. Of course, the associated enhancement of the tails of the distribution by the nonhermitean FSI is also seen. Thus, Fig. 16 provides a more direct confirmation of the characterization of nonhermitean effects inferred from Figs. 13-15. Although the gross features of quasielastic electron scattering can be mimicked by modifications to purely hermitean, energy-independent FSI, additional nontrivial features are produced by a realistic complex optical potential. For a microscopic description of the quasielastic response it is necessary to properly incorporate the reactive content represented by the nonhermiticity and energy dependence of the optical potential.

V. Summary and Conclusions

In this paper a microscopic theoretical, Green's-function formalism for analyzing the response functions of the inclusive quasielastic (e, e') reaction has been reviewed, developed and applied. This formalism properly incorporates the nonhermitean potentials needed to reflect inelastic multistep and absorptive processes. The Green's function formalism provides a conceptually clear framework for treating the quasielastic inclusive reaction that goes far beyond simple plane-wave or Hermitean potential models, permitting a relatively clear identification of approximations and appropriate corrections. The formalism also provides an advantageous numerical framework for analyzing FSI, relativistic dynamics and other mechanisms relevant to inclusive quasielastic (e, e'). A number of relativistic and nonrelativistic dynamical models of the final state interactions have been examined for the

case of ^{40}Ca . This was done in a manner which allowed for the isolation of several distinct dynamical mechanisms. A number of conclusions can be inferred from these investigations.

1. FSI effects can never be neglected or approximated away. For meaningful comparisons with the data, FSI are essential; plane-wave approximations are never adequate. The FSI serve to suppress the heights of the peaks for both quasielastic response functions and transfer strength to the tails of the distributions. Off-shell scattering dynamics, which is not well constrained by elastic proton scattering, determines the q - ω distribution of approximately 50 percent of the response functions. Differing off-shell behaviors of the optical potentials result in significant modifications to the response functions: off-shell FSI are invariably important.

2. The reactive content of the optical potentials, which is manifested in the energy dependence and nonhermiticity of the optical potentials, is important to the description of the response functions. Hermitean, energy-independent potentials, such as the Hartree potential, fail to produce the appropriate shape for the response functions. This defect becomes more pronounced with increasing momentum transfer. Hermitean, energy-independent potentials transfer insufficient strength to the high energy tails of the response functions. Energy-dependent, nonhermitean optical potentials provide a much more realistic and physically appropriate analysis of quasielastic electron scattering.

3. Since FSI suppress both R_L and R_T , the transverse response must be enhanced by physical mechanisms which are not included in the one-body optical model. This is supported by recent experimental and theoretical work in the $(e, e'p)$ reaction.^{46,47} The transverse anomaly cannot be used to justify the plane-wave approximation nor should models which do not incorporate FSI suppression of the transverse response relative to the plane wave result be considered advantageous.

4. Relativistic negative-energy contributions, which are the new dynamical degrees of freedom included in the Dirac FSI, result in greater suppression of the longitudinal response than the transverse response. For the nonrelativistic FSI, the predicted suppression of the two response functions is roughly the same. Half of the additional "relativistic" suppression of the longitudinal quasielastic peak, and all of the additional "relativistic" suppression of the transverse peak, arises not from pair effects but from nonrelativistic-type off-shell differences in the optical

potential. The effects of explicit and implicit negative-energy "pair" contributions are of approximately the same magnitude; both suppress the longitudinal response while the two contributions tend to cancel for the transverse response. Thus pair effects double the additional relativistic suppression of the longitudinal response, but have little impact on the transverse response. The negative-energy components of the bound state wave functions have a negligible effect on the response functions.

5. The longitudinal response functions calculated with relativistic dynamical FSI have the appropriate shape, but the suppression is inadequate to account for the available data. No parameter-free description of the FSI was found able to simultaneously describe existing experimental data for both the longitudinal and transverse quasielastic response functions.

Support of the U. S. Department of Energy and the University of Maryland Computer Science Center for this research is gratefully acknowledged.

Appendix A

This appendix extends the unsymmetrized formalism (7)-(19) of the text to properly reflect the full implications of the Pauli principle. The purposes of this are [1] to provide a fully antisymmetrized formal development, [2] to show that all of the main results of the text, namely (16)-(19), are consistent with the fully antisymmetrized development, and [3] to point out some interesting theoretical points that arise as a result of the Pauli principle.

Given (9) we wish to connect the operator $P_{\alpha_1} \hat{G} P_{\alpha_1}$ to the optical theory as before. First the ejectile-nucleus antisymmetrization operator \hat{A} is introduced, where \hat{A} is a full A-particle antisymmetrizer normalized according to

$$\hat{A}^2 = A \hat{A} \quad , \quad (\text{A.1})$$

so that

$$\Lambda = \hat{A}/A \quad , \quad (\text{A.2})$$

is the usual projection operator onto antisymmetric states

$$\Lambda^2 = \Lambda \quad . \quad (\text{A.3})$$

The antisymmetrization requirement on \hat{G} is made explicit in (9) by replacing

$$P_{\alpha_1} \hat{G} P_{\alpha_1} \rightarrow P_{\alpha_1} \hat{\Lambda} \hat{G} P_{\alpha_1} \quad , \quad (\text{A.4})$$

so that (9) becomes

$$T^{uv} \approx \bar{\sum}_i \sum_{\alpha_1} \langle i | \hat{J}^v(q)^\dagger P_{\alpha_1} \hat{\Lambda} \hat{G} P_{\alpha_1} \hat{J}^v(q) | i \rangle \quad . \quad (\text{A.5})$$

This follows, for example, by replacing \hat{G} by $\hat{\Lambda} \hat{G}$ in (5) and carrying it forward to (9). Now from the resolvent identity

$$\hat{G} \hat{A} = G_{\alpha_1} \hat{A} + G_{\alpha_1} V^{\alpha_1} \hat{A} \hat{G} \quad (\text{A.6})$$

$$= G_{\alpha_1} + G_{\alpha_1} T_{\text{ACS}}^{\alpha_1} G_{\alpha_1} \quad (\text{A.7})$$

where $T_{\text{ACS}}^{\alpha_1}$ is the Alt-Grassberger-Sandhas (AGS) form of the antisymmetrized

transition operator⁴⁸

$$T_{\text{ACS}}^{\alpha_1} = G_{\alpha_1}^{-1} \hat{G} \hat{A} G_{\alpha_1}^{-1} - G_{\alpha_1}^{-1} \quad , \quad (\text{A.8a})$$

$$= V_{\alpha_1}^{\hat{A} \hat{G}} G_{\alpha_1}^{-1} + (\hat{A} - 1) G_{\alpha_1}^{-1} \quad . \quad (\text{A.8b})$$

If we now make the replacements (11) \rightarrow (A.6), (13) \rightarrow (A.8), make use of the definitions (12) and (14), and replace $(1/A)\Sigma \rightarrow \sum_{\alpha_1}$, where the latter sum

runs over physically distinct channels, (16) is recovered where now $V_{\text{opt}}^{\alpha_1}$ is the AGS-based optical potential of refs. 28 and 29. It is not at all surprising that it is this optical potential which should arise here.^{28,30} In fact, (A.8a) is Hermitean analytic so that the associated optical potential is Hermitean analytic as well. Thus the unitarity and dispersion relations (17)-(19) are also recovered in the same form as in the text.

In contrast, the optical potential based on the more usual "prior" form of the antisymmetrized transition operator, which is just the first term on the right-hand side of (A.8b), is not Hermitean analytic and hence neither is its associated optical potential. Because of this, discontinuity and unitarity relations do not coincide and relation (19) is not obeyed. This is of interest because the multiple scattering theoretic basis for high-energy approximations to the optical potential is derived on the basis of the prior form of the T-matrix³¹ [See, however, Ref. 30 for a multiple scattering series based on $T_{\text{ACS}}^{\alpha_1}$].

It is interesting that the result of this appendix implies that, at least in principle, (16) requires the use of the optical potential based upon the AGS form for T, in distinction from other off-shell extensions of T. From ((A.6) - (A.8)) this is connected to the spectral decomposition of \hat{G} and thus to the Coulomb sum rule, as well as to the analytic structure of $V_{\text{opt}}^{\alpha_1}$. Since the optical potential based on $T_{\text{ACS}}^{\alpha_1}$ is free of the elastic α_1 -channel unitary cut whereas the prior-based optical potential is not,²⁸⁻³⁰ this dichotomy carries over at least formally to the Coulomb sum rule within the context of the one-body optical model.

REFERENCES

- 1.) E. J. Moniz, Phys. Rev. 184, 1154 (1969); A. L. Fetter and J. D. Walecka, *Quantum Theory of Many Particle Systems* (McGraw-Hill, New York, 1971), pp. 192-194.
- 2.) E. J. Moniz, *et al.*, Phys. Rev. Lett. 26, 445 (1971); R. R. Whitney, *et al.*, Phys. Rev. C 9, 2230 (1974); J. W. Van Orden, Ph. D. Thesis, Stanford University (1978), unpublished.
- 3.) Z. E. Meziani, *et al.*, Phys. Rev. Lett. 52, 2130 (1984); Z. E. Meziani, *et al.*, Phys. Rev. Lett. 54, 1233 (1985); Z. E. Meziani, *et al.*, Nucl. Phys. A46, 113c (1985).
- 4.) M. Deady, *et al.*, Phys. Rev. C 33, 1897 (1986) and M. Deady, *et al.*, Phys. Rev. C 28, 631 (1983).
- 5.) C. C. Blatchley, *et al.*, Phys. Rev. C 34, 1243 (1986); B. Frois, Nucl. Phys. A434, 57 (1985); A. Hotta, *et al.*, Phys. Rev. C 30, 87 (1984); P. Barreau, *et al.*, Nucl. Phys. A402, 515 (1983); P. Barreau, *et al.*, Nucl. Phys. A358, 287c (1981); R. Altemus, *et al.*, Phys. Rev. Lett. 44, 965 (1980).
- 6.) U. Stroth, R. W. Hasse and P. Schuck, Nucl. Phys. A462, 45 (1987) and Phys. Lett. B171, 339 (1986); W. M. Alberico, A. Molineri, A. De Pace, M. Ericson and M. B. Johnson, Phys. Rev. C 34, 977 (1986); F. A. Brieva and A. Dellafiore, Phys. Rev. C 36, 899 (1987); G. Co' and S. Krewald, Nucl. Phys. A433, 392 (1985); M. Cavinato, *et al.*, Nucl. Phys. A423, 376 (1984).
- 7.) G. Co', K. Quader and J. Wambach, "Second Workshop on Problems of Theoretical Nuclear Physics", Cortona, Italy, Oct. 5-7, 1987; S. Drożdż, G. Co', J. Wambach and J. Speth, Phys. Lett. B185, 287 (1987).
- 8.) G. Do Dang, M. L'Huillier, N. Van Giai, J. W. Van Orden, Phys. Rev. C 35, 1637 (1987); G. Orlandini and M. Traini, Phys. Rev. C 31, 280 (1985); see also Ref. 4.
- 9.) H. Kurasawa and T. Suzuki, Phys. Lett. B208, 160 (1988) and Phys. Lett. B211, 500E (1988); J. V. Nobel, Phys. Lett. B178, 285 (1986) and Phys. Rev. Lett. 46, 412 (1981); L. S. Celenza, A. Rosenthal and C. M. Shakin, Phys. Rev. Lett. 53, 892 (1984) and Phys. Rev. C 31, 232 (1985).

- 10.) P. J. Mulders, Phys. Rev. Lett. 54, 2560 (1985) and Nucl. Phys. A459, 525 (1986).
- 11.) R. Rosenfelder, Ann. Phys. (N.Y.) 128, 188 (1980).
- 12.) G. Do Dang and Nguyen Van Giai, Phys. Rev. C 30, 731 (1984); S. Nashizaki, H. Kurasawa, & Toshio Suzuki, Phys. Lett. 171B, 1 (1986); S. Nishizaki, T. Maruyama, H. Kurasawa, T. Suzuki, Nuc. Phys. A485, 515 (1988). 13.) R. Brockmann, private communication.
- 14.) K. Wehrberger and F. Beck, Phys. Rev. C 35, 298 (1987) and Phys. Rev. 37, 1148 (1988); H. Kurasawa and T. Suzuki, Nucl. Phys. A454, 527 (1986) and Kyoto Univ. preprint RIFP-739, MIT preprint CTP#1589, MIT preprint CTP#1601.
- 15.) C. J. Horowitz, Indiana University preprint IU/NTC 88-4 and proceedings of the Workshop on Relativistic Nuclear Many-Body Physics, Columbus, Ohio, June 1988; J. R. Shepard, proceedings of the Workshop on Relativistic Nuclear Many-Body Physics, Columbus, Ohio, June 1988; Xiangdong Ji, California Institute of Technology preprint.
- 16.) Y. Kawazoe, G. Takeda and H. Matsuzaki, Prog. of Theo. Phys., 54, 1394 (1975); S. Klawansky, *et al.*, Phys. Rev. C 7, 795 (1973); T. W. Donnelly, Nucl. Phys. A150, 393 (1970); T. DeForest, Jr., Nucl. Phys. A132, 305 (1969). 17.) Y. Horikawa, F. Lenz and Nimai C. Mukhopadhyay, Phys. Rev. C 22, 1680 (1980). 18.) J. J. Kelly, *et al.*, "Density Dependence in the Two-Nucleon Effective Interaction at 135 MeV", Phys. Rev. C, to be published; J. J. Kelly, "Complementarity Between Electromagnetic and Hardronic Probes of Nuclear Structure", invited contribution to "Critical Relationships between Structure and Reactions in Nuclear Physics", (Drexel University, September 15-18, 1986).
- 19.) H. Feshbach, Ann. Phys. 5, 357 (1958) and Ann. Phys. 19, 287 (1962).
- 20.) P. Schwandt, *et al.*, Phys. Rev. C 26, 55 (1982).
- 21.) K. Nakayama and W. G. Love, Phys. Rev. C 38, 51 (1988).
- 22.) A. Picklesimer, P. C. Tandy, R. M. Thaler, and D. H. Wolfe, Phys. Rev. C 29, 1582 (1984) and Phys. Rev. C 30, 1861 (1984).
- 23.) M. V. Hynes, A. Picklesimer, P. C. Tandy, and R. M. Thaler, Phys. Lett. 52, 978 (1984) and Phys. Rev. C 31, 1438 (1985).
- 24.) See, for example, H. Feshbach, Ann. Rev. Nucl. Sci., 8, 49 (1958), Ref. 19 and Ref. 28.
- 25.) See, for example, P. Schwandt, F. Petrovich, and A. Picklesimer, IUCF Technical and Scientific Report, December, 1978, p. 27.

- 26.) J. A. McNeil, J. R. Shepard and S. J. Wallace, Phys. Rev. Lett. 50, 1429 (1983); J. R. Shepard, J. A. McNeil and S. J. Wallace, Phys. Rev. Lett. 50, 1443 (1983); B. C. Clark, S. Hama, R. L. Mercer, L. Ray and B. D. Serot, Phys. Rev. Lett. 50, 1644 (1983).
- 27.) E. D. Cooper, *et al.*, Phys. Rev. C 36, 2170 (1987) and E. D. Cooper, B. C. Clark, S. Hama and R. L. Mercer, Phys. Lett. B206, 588 (1988).
- 28.) K. L. Kowalski and A. Picklesimer, Phys. Rev. Lett. 46, 228 (1981) and Nucl. Phys. A369, 336 (1981).
- 29.) R. Goldflam and K. L. Kowalski, Phys. Rev. Lett. 44, 1044 (1980) and Phys. Rev. C 22, 949 (1980).
- 30.) A. Picklesimer, Phys. Rev. C 24, 1400 (1981).
- 31.) E. R. Siciliano and R. M. Thaler, Phys. Rev. C 16, 1322 (1977); A. Picklesimer and R. M. Thaler, Phys. Rev. C 23, 42 (1981).
- 32.) C. J. Horowitz and B. D. Serot, Nucl. Phys. A368, 503 (1981).
- 33.) T. DeForest, Jr. and J. D. Walecka, Advances in Physics 15, 1 (1966); T. W. Donnelly and J. D. Walecka, Ann. Rev. Nucl. Sci. 25, 729 (1975).
- 34.) J. D. Bjorken and S. D. Drell, *Relativistic Quantum Mechanics* (McGraw-Hill, New York, 1964).
- 35.) More generally, the simplification introduced by Eq. (8) is not needed for this result.
- 36.) Formally, this assumes that the optical potential is Hermitean analytic.
- 37.) A. Picklesimer, J. W. Van Orden and S. J. Wallace, Phys. Rev. C 32, 1312 (1985).
- 38.) See, for example, P. Stichel and E. Werner, Nucl. Phys. A145, 257 (1970); M. Chemtob and M. Rho, Nucl. Phys. A163, 1 (1971); M. Gari and H. Hyuga, Z. Phys. A277, 291 (1976); W. Jaus and W. Woolcock, Nucl. Phys. A431, 669 (1984); J. L. Friar and W. C. Haxton, Phys. Rev. C 31, 2027 (1985); W. M. Alberico, R. Cenni, A. Molinari and P. Saracco, Ann. Phys. 174, 131 (1987).
- 39.) A. J. F. Siegert, Phys. Rev. 52, 787 (1937); J. L. Friar and S. Fallieros, Phys. Lett. 114B, 403 (1982) and Phys. Rev. C 29, 1645 (1984).
- 40.) See, for example, A. Gal, G. Toker, and Y. Alexander, Ann. Phys. (N.Y.) 137, 341 (1981).
- 41.) G. Höhler, *et al.*, Nucl. Phys. B114, 505 (1976).
- 42.) J. L. Friar, private communication.
- 43.) C. R. Chinn, A. Picklesimer, and J. W. Van Orden, to be published.

- 44.) M. A. Franey and W. G. Love, Phys. Rev. C 31, 488 (1985).
- 45.) A. Dellafiore, F. Lenz and F. A. Brieva, Phys. Rev. C 31, 1088 (1985);
see also Ref. 17.
- 46.) See also, P. E. Ulmer, *et al.*, Phys. Rev. Lett. 59, 2259 (1987)
- 47.) A. Picklesimer and J. W. Van Orden, Phys. Rev. C, to be published
- 48.) E. O. Alt, P. Grassberger, and W. Sandhas, Nucl. Phys. B2, 167 (1967);
P. Grassberger and W. Sandhas, Nucl. Phys. 132, 181 (1967).

Figure Captions

- Fig. 1 : Diagram of the final state interaction contribution to the forward virtual Compton amplitude, which is the scattering of virtual photons from a nucleon in the nucleus. The "T" represents the final state interaction between the ejectile and the residual nucleus. J^μ and J^ν are photonuclear electromagnetic vertices.
- Fig. 2 : The longitudinal (a.) and transverse (b.) response functions for ^{40}Ca at $q = 410 \text{ MeV}/c$ as a function of energy transfer, ω . Calculations are shown for the free relativistic plane wave approximation with no final state interactions (dotted line), the nonrelativistic LDA with Bonn N-N amplitudes (solid line), the nonrelativistic IA with Franey-Love N-N amplitudes (dot-dash line), the nonrelativistic optimally factorized IA with Franey-Love amplitudes (short-dash line), and the nonrelativistic Woods-Saxon fit (long-dash line). The data are from ref. 4 (solid diamonds) and ref. 3 (open boxes).
- Fig. 3 : (3a.) and (3b.) are the same as in Fig. 2 except at $q = 550 \text{ MeV}/c$. Figs. 3c and 3d are the same as 3a and 3b, respectively, except only the on-shell contributions from T_{opt} are included in the calculations.
- Fig. 4 : Longitudinal (a.) and transverse (b.) response functions for ^{40}Ca at $q = 410 \text{ MeV}/c$ as a function of energy transfer, ω . Calculations are shown for the relativistic free plane wave approximation (dotted line), Dirac global phenomenology (long-dash line) and the Dirac IA (short-dash line). On-shell curves are also displayed, where Dirac global phenomenology (dot-long-dash line) and the Dirac IA (dot-short-dash line) are used.
- Fig. 5 : The same as Fig. 4, except at $550 \text{ MeV}/c$ momentum transfer.

Fig. 6 : Longitudinal (a.) and transverse (b.) response functions for ^{40}Ca at $q = 410 \text{ MeV}/c$ as a function of energy transfer, ω . Calculations are shown for the relativistic free plane wave approximation (dotted line), Dirac global phenomenology (long-dash line) and the nonrelativistic LDA with Bonn N-N amplitudes (short-dash line). On-shell curves are also displayed for the Dirac global phenomenology (dot-long-dash line) and the nonrelativistic LDA with Bonn (dot-short-dash line).

Fig. 7 : The same as Fig. 6, except at $550 \text{ MeV}/c$ momentum transfer.

Fig. 8 : Longitudinal (a.) and transverse (b.) response functions for ^{40}Ca at $q = 410 \text{ MeV}/c$ as a function of energy transfer, ω . Calculations are shown for the relativistic free plane wave approximation (dotted line), the Dirac (long-dash line) and nonrelativistic (short-dash line) optimally factorized IA with Franey-Love amplitudes. On-shell curves are also displayed for the Dirac (dot-long-dash line) and nonrelativistic IA with Franey-Love amplitudes (dot-short-dash line).

Fig. 9 : The same as Fig. 8, except at $550 \text{ MeV}/c$ momentum transfer.

Fig. 10 : Longitudinal (a.) and transverse (b.) response functions for ^{40}Ca at $q = 410 \text{ MeV}/c$ as a function of energy transfer, ω . The relativistic free plane wave approximation (dotted line) calculation is shown along with calculations using Dirac global phenomenology to describe the FSI. The full Dirac calculation (long-dash line), the pure positive-energy NP calculation (short-dash line), and the NEP calculation with no explicit negative-energy terms in eq. (31) (solid line) are shown along with on-shell calculations with (dot-long-dash line) and without (dot-short-dash line) negative-energy contributions.

Fig. 11 : The same as Fig. 10, except at $550 \text{ MeV}/c$ momentum transfer.

Fig. 12 : The same as Fig. 10 and 11, except at $700 \text{ MeV}/c$ momentum transfer.

Fig. 13 : Longitudinal (a.) and transverse (b.) response functions for ^{40}Ca at $q = 410 \text{ MeV}/c$ as a function of energy transfer, ω . The relativistic free plane wave approximation calculation (dotted line) is shown along with calculations using Dirac global phenomenology in full Dirac (long-dash line) and positive-energy NP (short-dash line) format, and using relativistic Hartree potentials in full Dirac (solid line) and positive-energy NP (dot-dash line) format.

Fig. 14 : The same as Fig. 13, except at $550 \text{ MeV}/c$ momentum transfer.

Fig. 15 : The same as Fig. 13, except at $700 \text{ MeV}/c$ momentum transfer.

Fig. 16 : Longitudinal (a.) and transverse (b.) response functions for ^{40}Ca at $q = 410 \text{ MeV}/c$ as a function of energy transfer, ω . The relativistic free plane wave approximation calculation (dotted line) is shown along with calculations using Dirac global phenomenology to describe the FSI. The full Dirac calculation (solid line) and a calculation, where only the real part of the same optical potential (dashed line) is used, are shown.

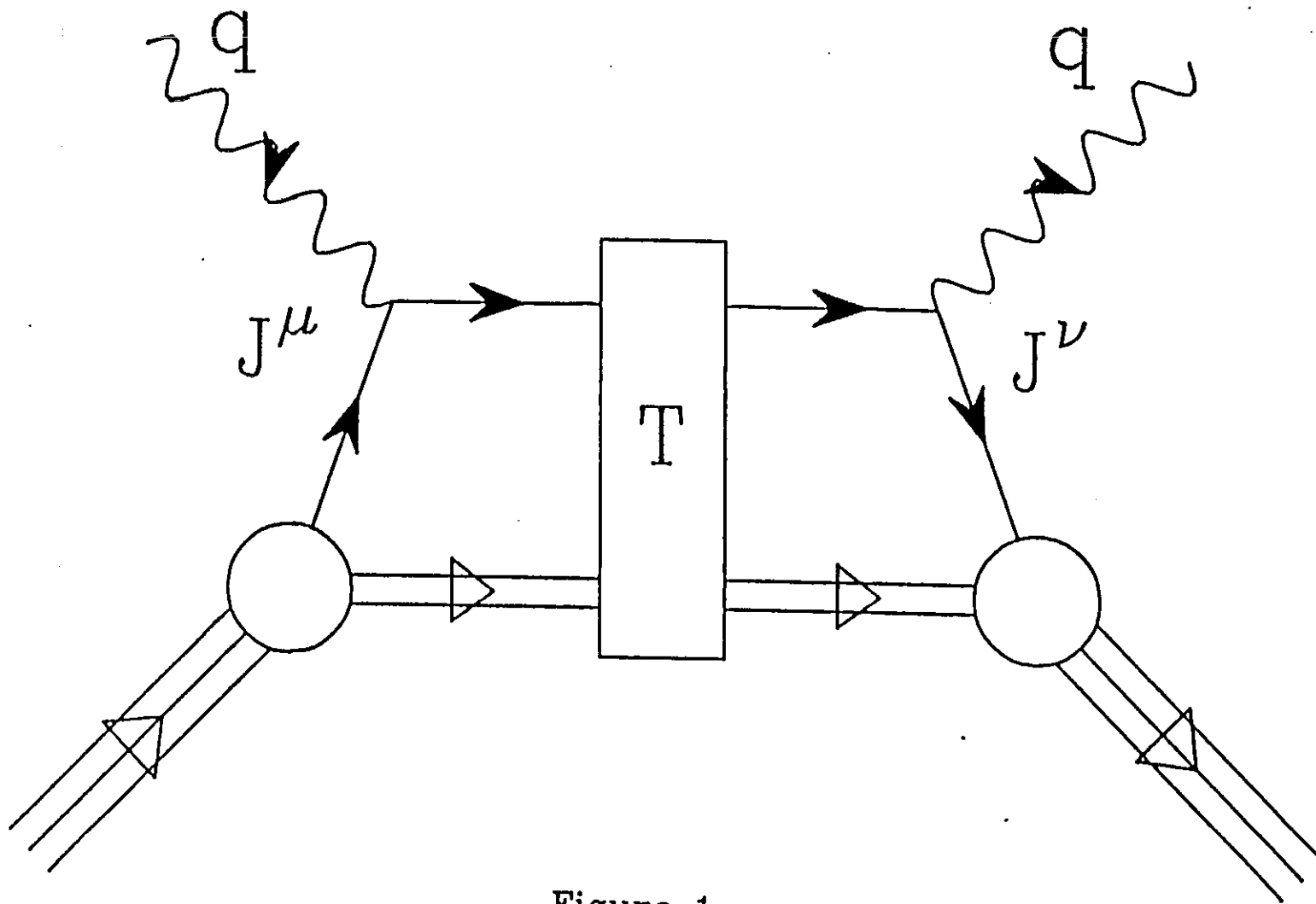


Figure 1

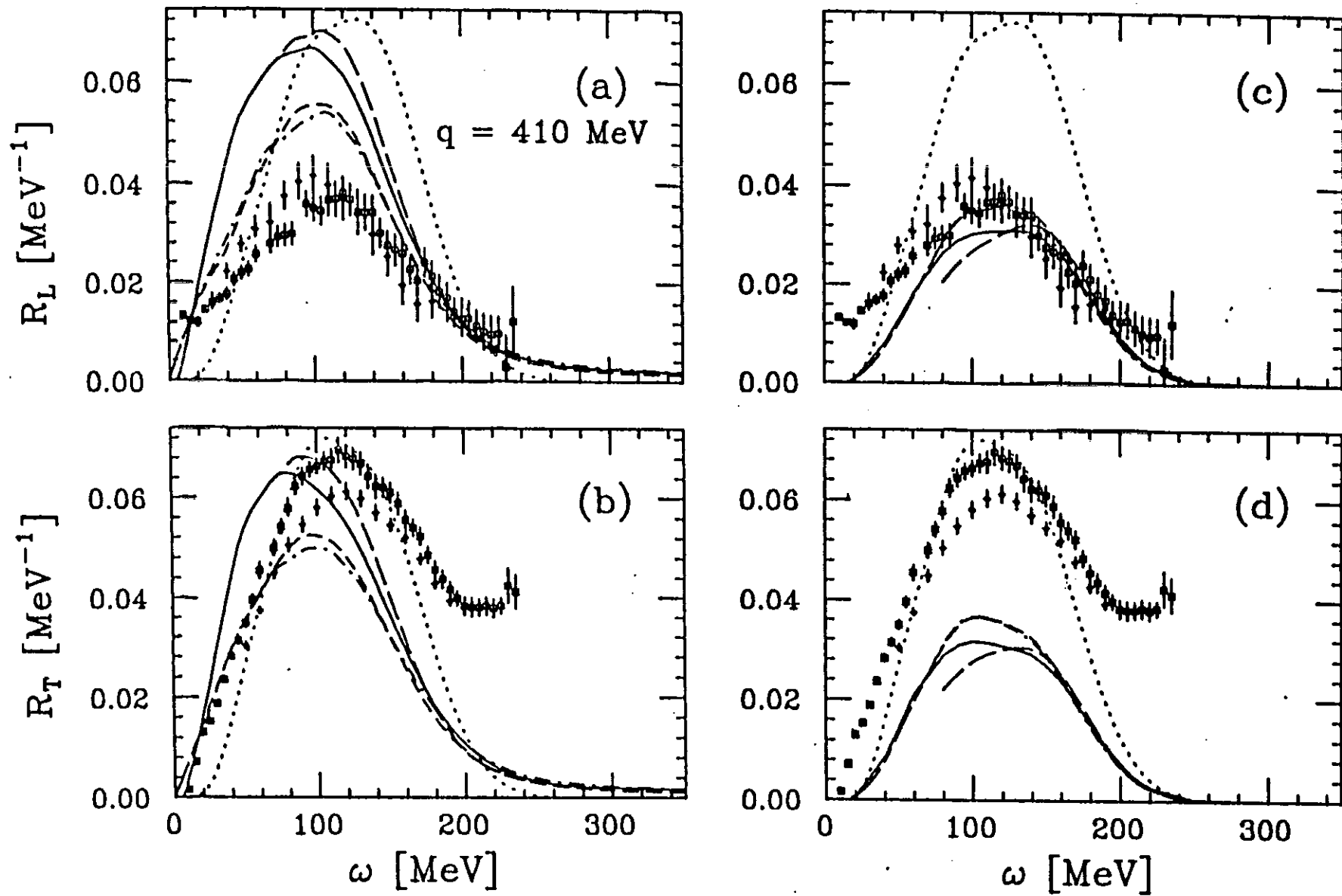


Figure 2

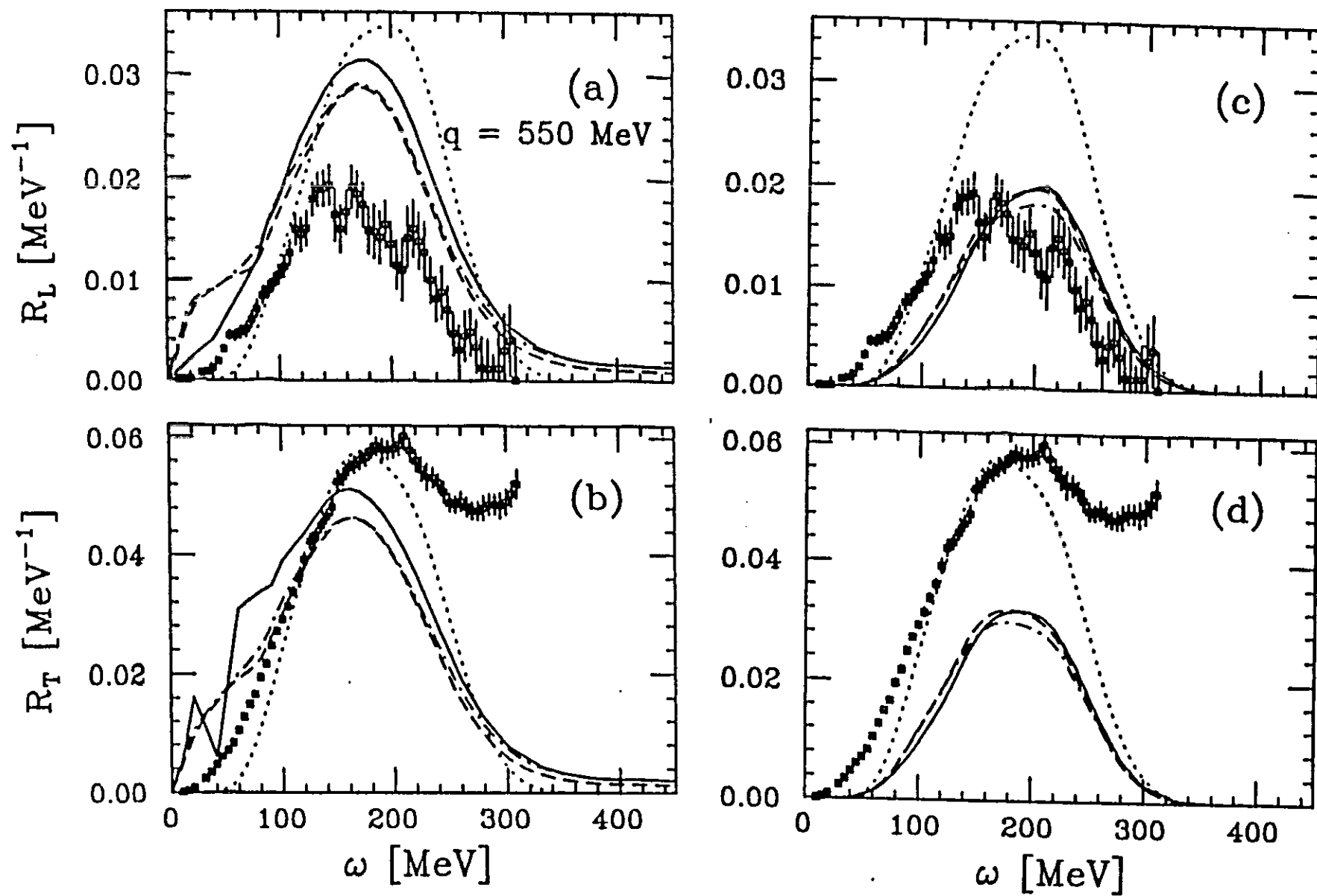


Figure 3

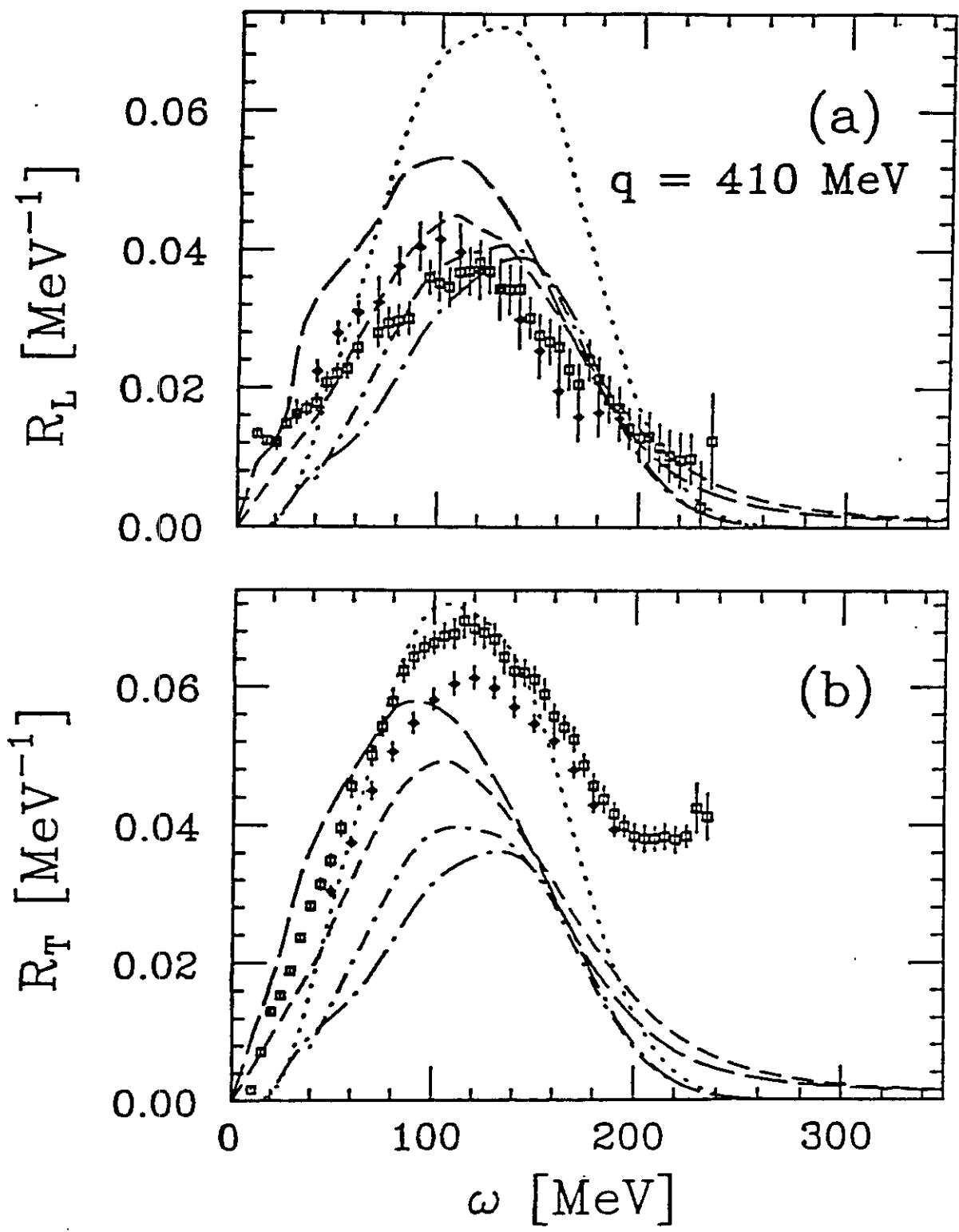


Figure 4

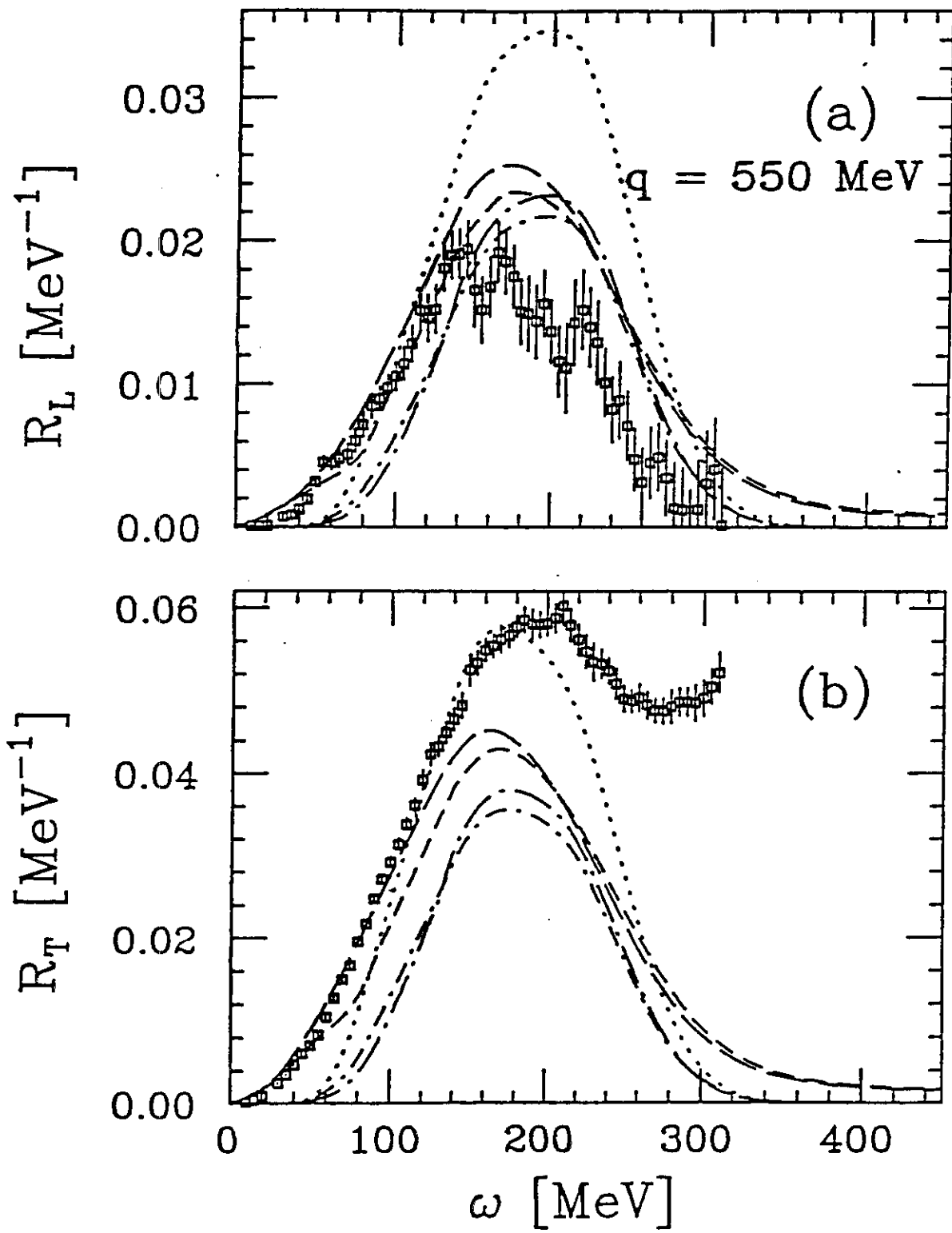


Figure 5

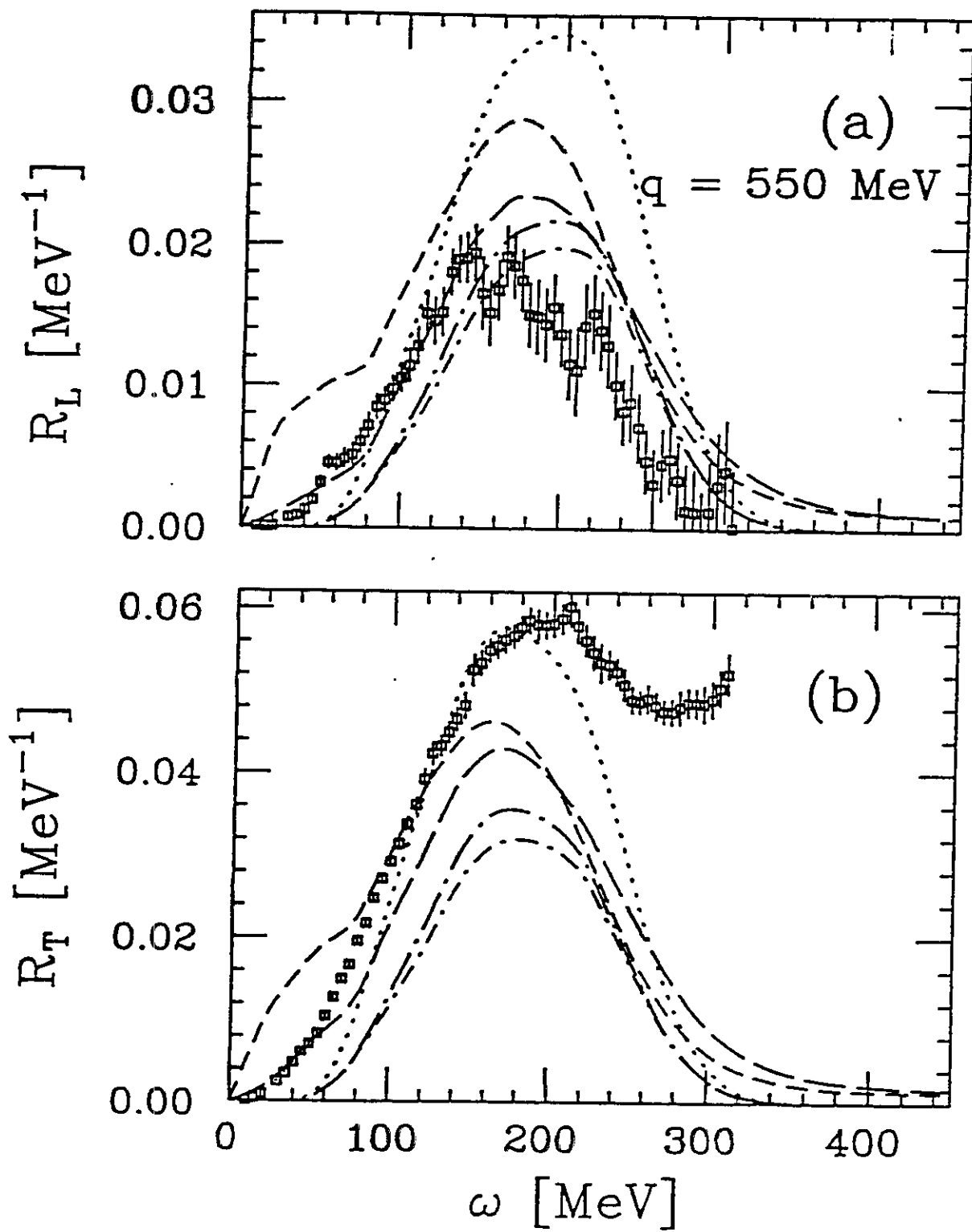


Figure 9

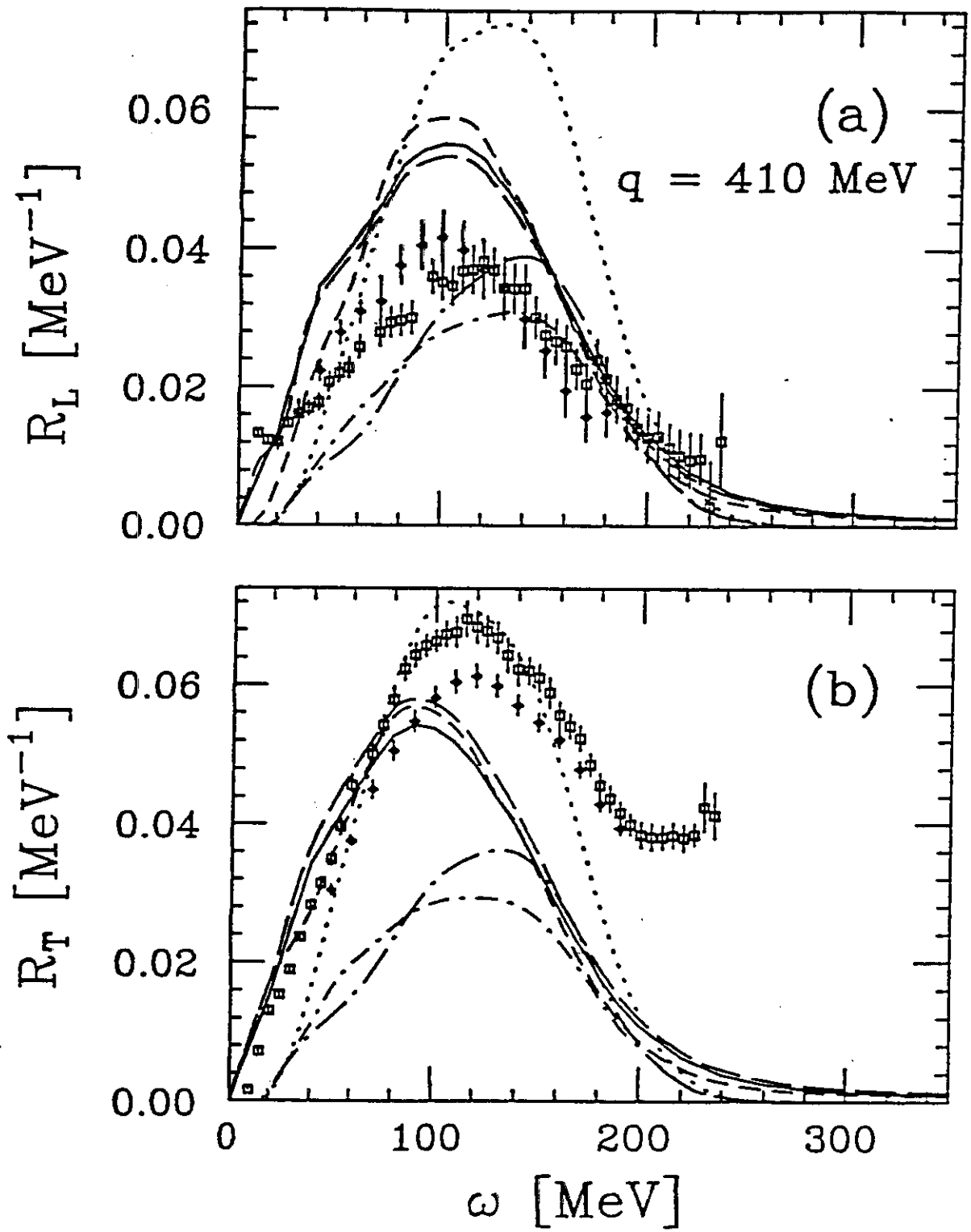


Figure 10

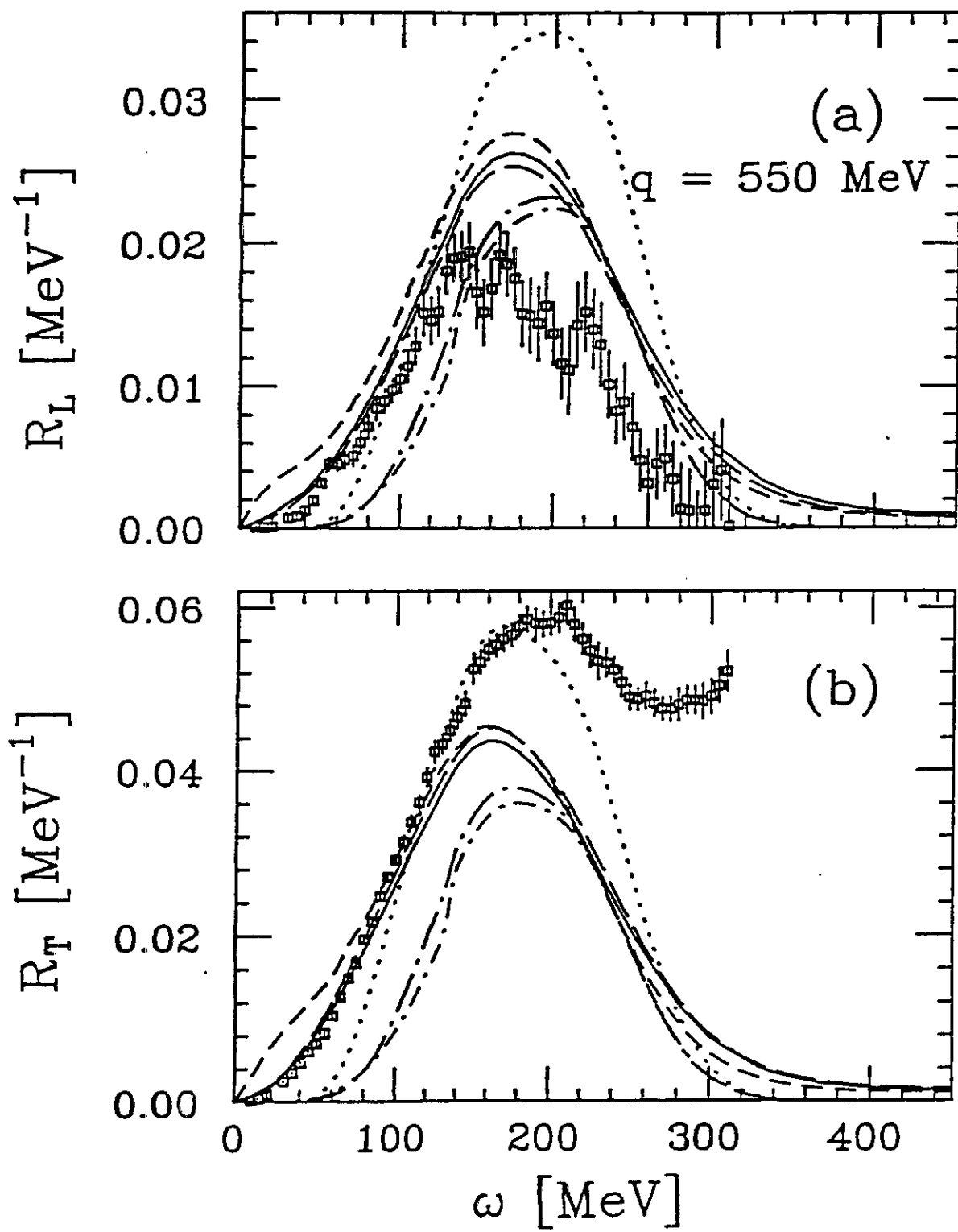


Figure 11

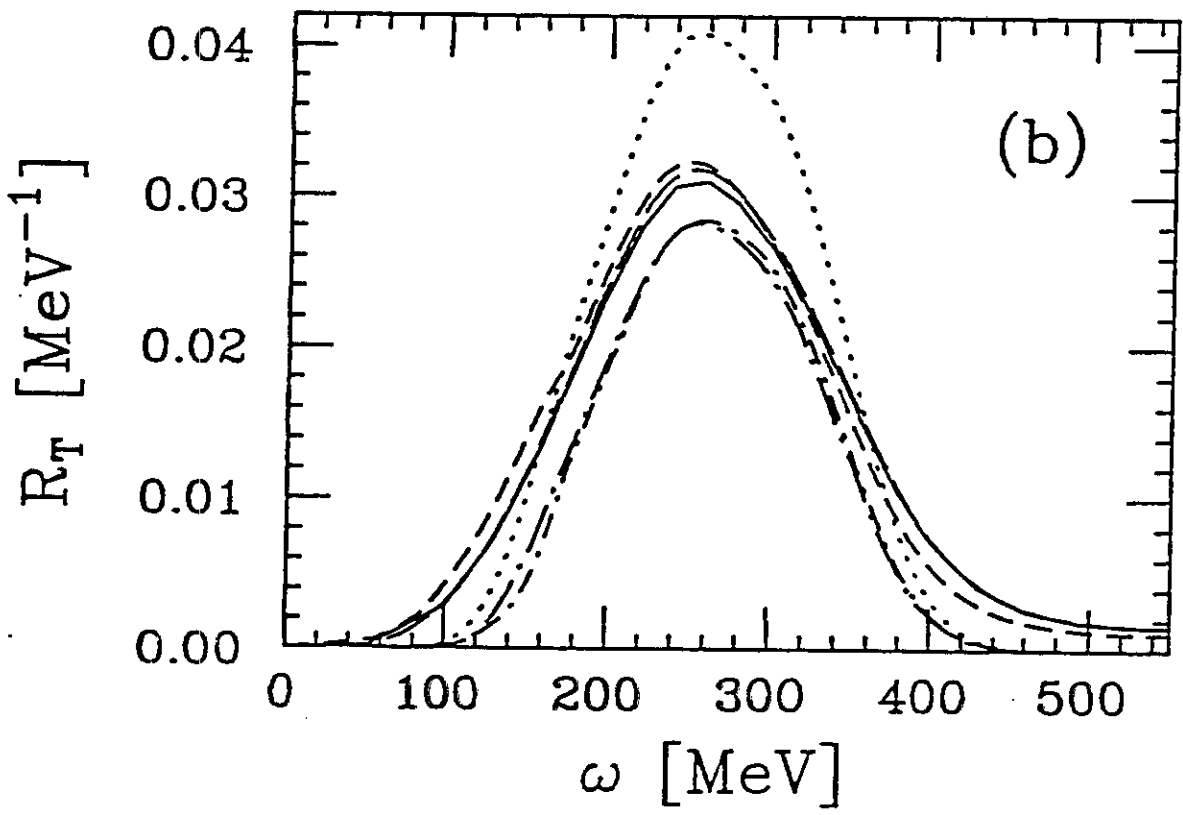
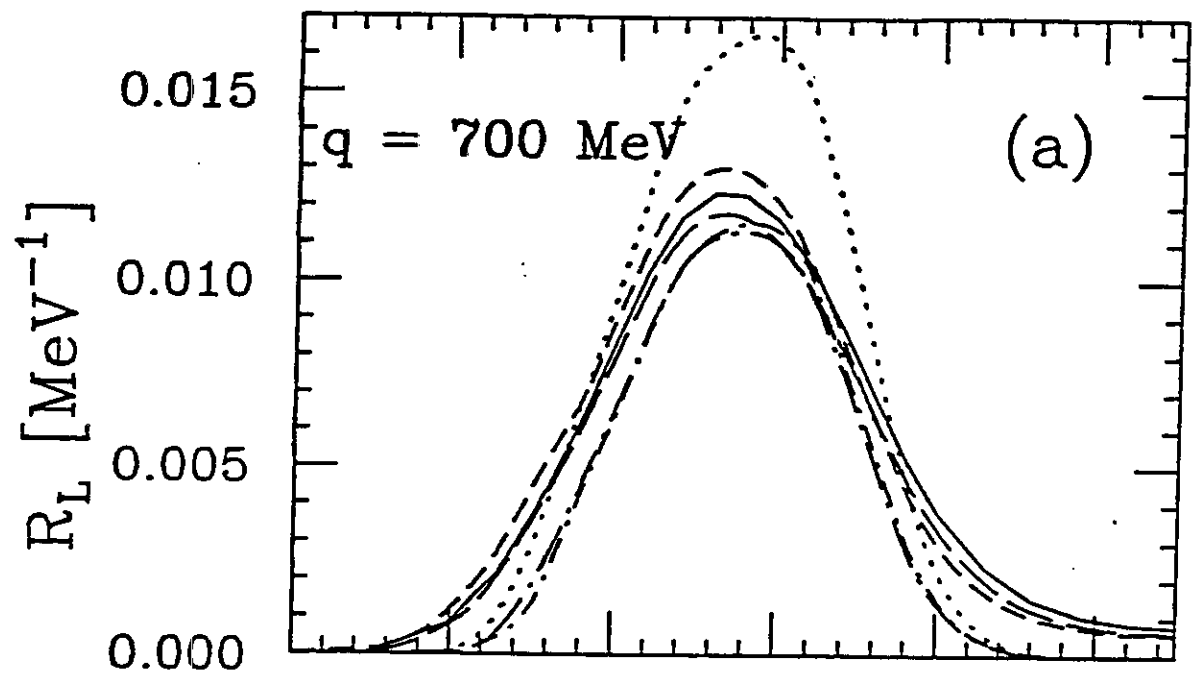


Figure 12

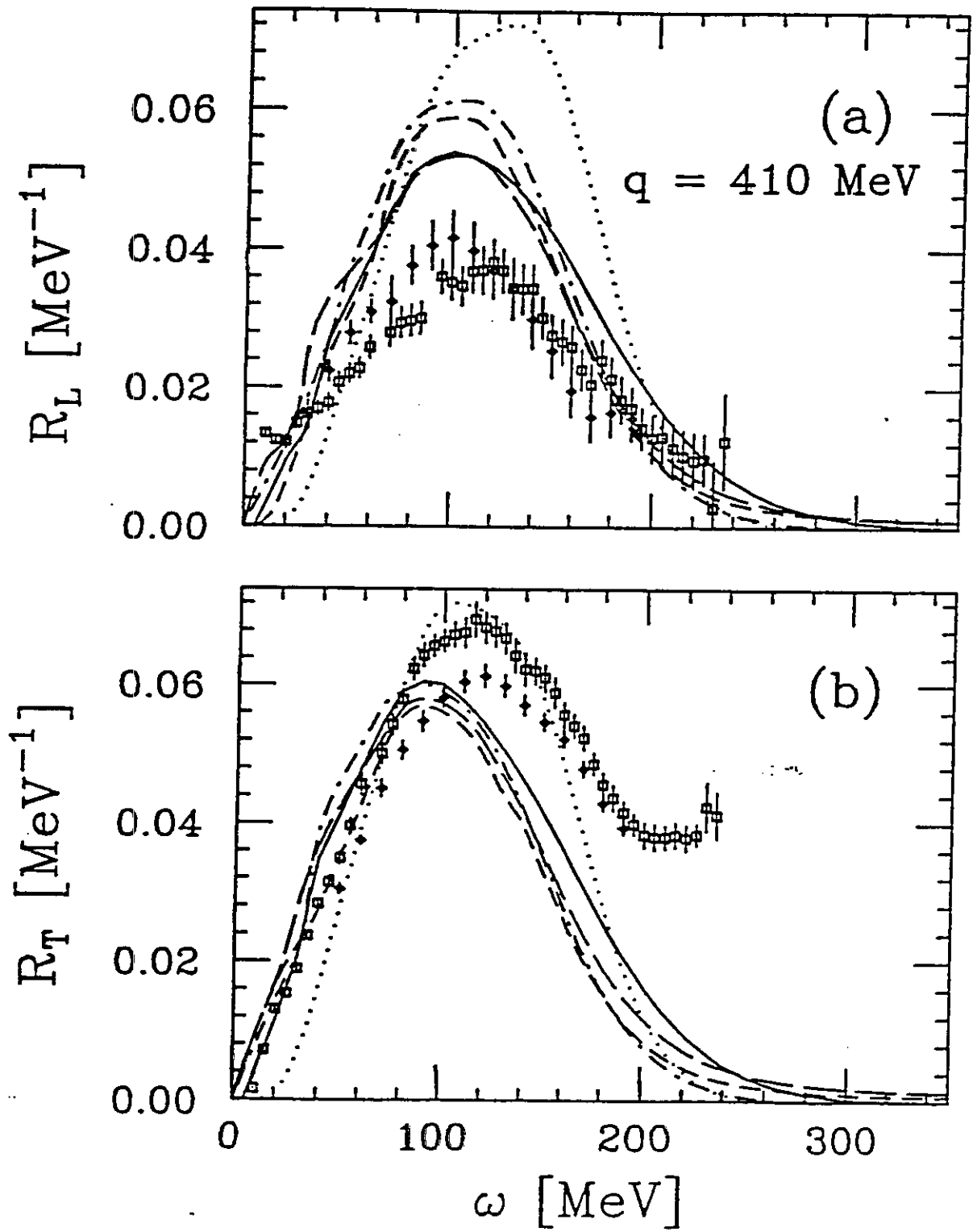


Figure 13

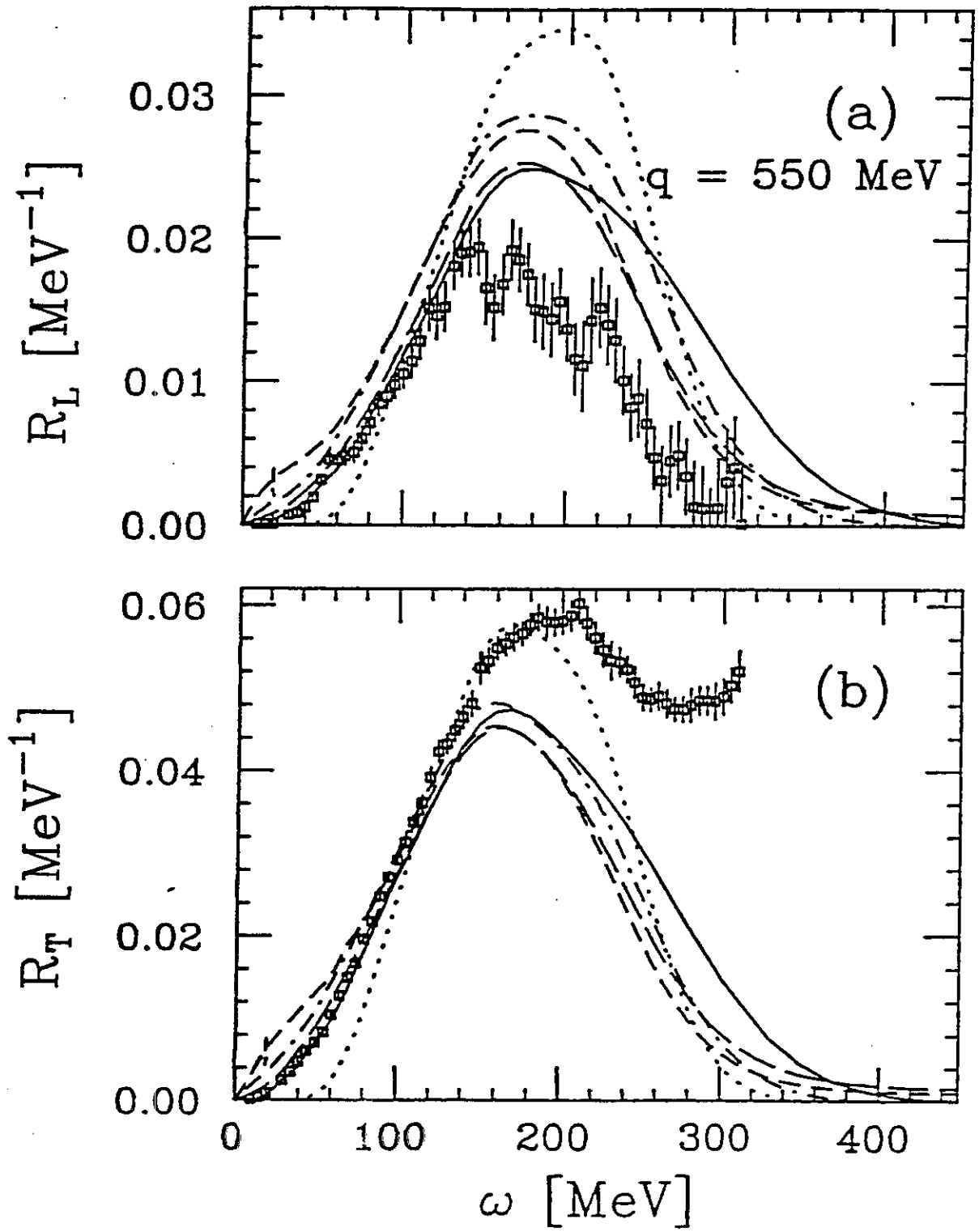


Figure 14

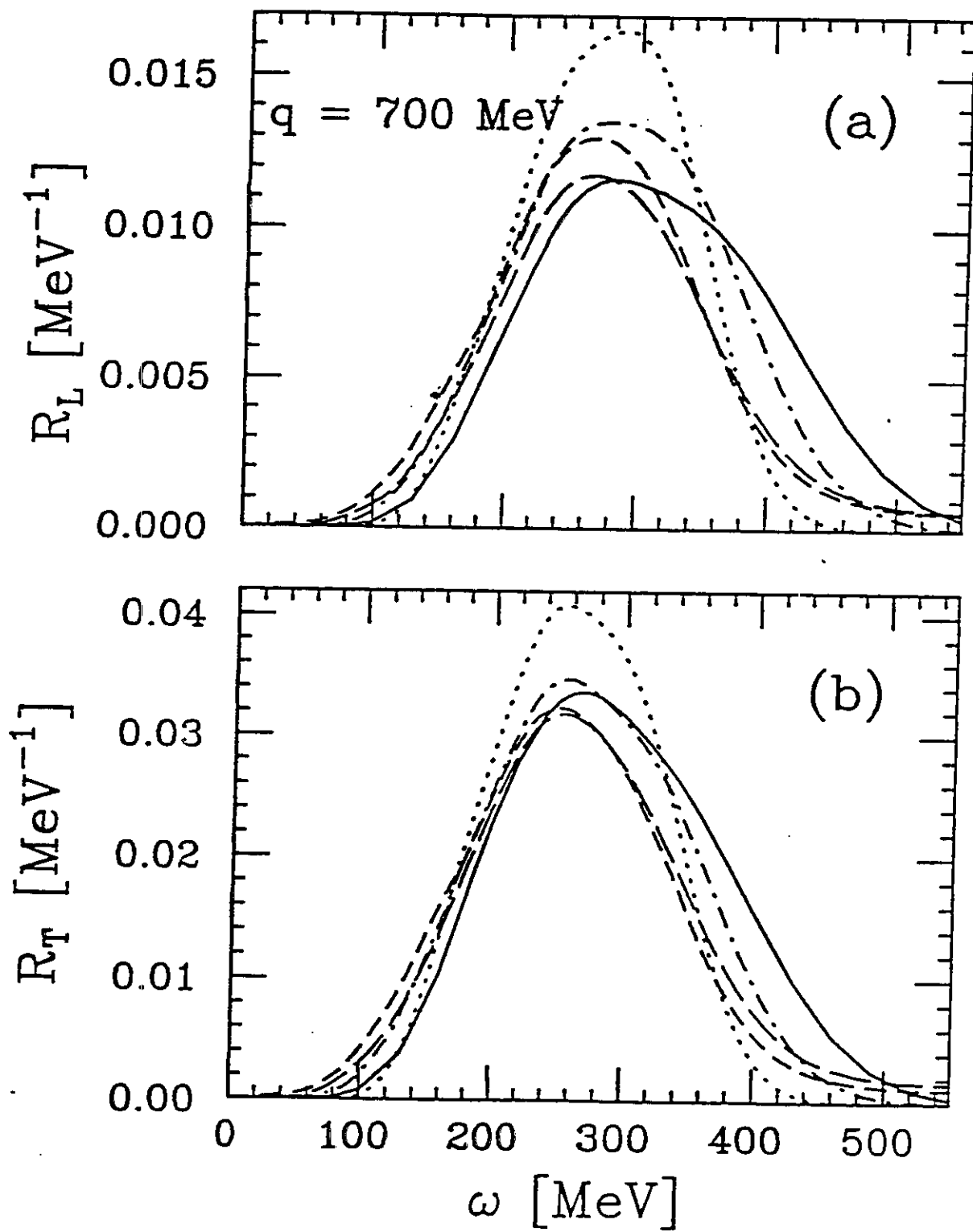


Figure 15

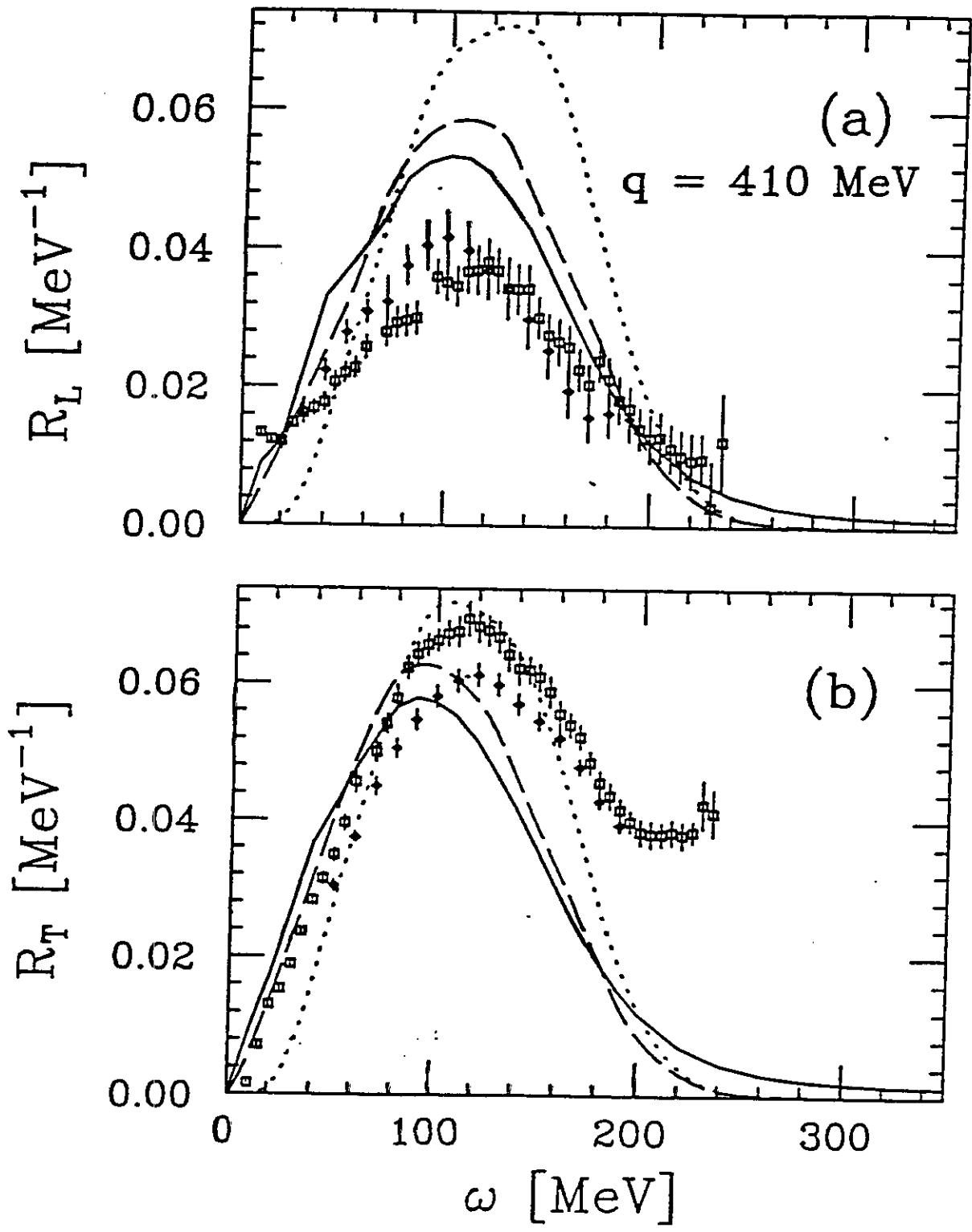


Figure 16